jove

Electromagnetic Source Imaging in Presurgical Evaluation of Children with Drug-Resistant Epilepsy

Ludovica Corona[1,2], **Sakar Rijal**[1,2], **Omer Tanritanir**[1], **Sadra Shahdadian**[1,2], **Cynthia G. Keator**[1], **Linh Tran**[1], **Saleem I. Malik**[1], **Madhan Bosemani**[1], **Daniel Hansen**[1], **Dave Shahani**[1], **M. Scott Perry**[1], **Christos Papadelis**[1,2,3]

[1] Neuroscience Research Center, Jane and John Justin Institute for Mind Health, Cook Children's Health Care System [2] Department of Bioengineering, University of Texas at Arlington [3] Burnett School of Medicine, Texas Christian University

Corresponding Author

Christos Papadelis

christos.papadelis@cookchildrens.org

Citation

Corona, L., Rijal, S., Tanritanir, O., Shahdadian, S., Keator, C.G., Tran, L., Malik, S.I., Bosemani, M., Hansen, D., Shahani, D., Perry, M.S., Papadelis, C. Electromagnetic Source Imaging in Presurgical Evaluation of Children with Drug-Resistant Epilepsy. *J. Vis. Exp.* (211), e66494, doi:10.3791/66494 (2024).

Date Published

September 20, 2024

DOI

10.3791/66494

URL

jove.com/video/66494

Abstract

For children with drug-resistant epilepsy (DRE), seizure freedom relies on the delineation and resection (or ablation/disconnection) of the epileptogenic zone (EZ) while preserving the eloquent brain areas. The development of a reliable and noninvasive localization method that provides clinically useful information for the localization of the EZ is, therefore, crucial to achieving successful surgical outcomes. Electric and magnetic source imaging (ESI and MSI) have been increasingly utilized in the presurgical evaluation of these patients showing promising findings in the delineation of epileptogenic as well as eloquent brain areas. Moreover, the combination of ESI and MSI into a single solution, namely electromagnetic source imaging (EMSI), performed on simultaneous high-density electroencephalography (HD-EEG) and magnetoencephalography (MEG) recordings has shown higher source localization accuracy than either modality alone. Despite these encouraging findings, such techniques are performed in only a few tertiary epilepsy centers, are rarely recorded simultaneously, and are underutilized in pediatric cohorts. This study illustrates the experimental setup for recording simultaneous MEG and HD-EEG data as well as the methodological framework for analyzing these data aiming to localize the irritative zone, the seizure onset zone, and eloquent brain areas in children with DRE. More specifically, the experimental setups are presented for (i) recording and localizing interictal and ictal epileptiform activity during sleep and (ii) recording visual-, motor-, auditory-, and somatosensory-evoked responses and mapping relevant eloquent brain areas (i.e., visual, motor, auditory, and somatosensory) during visuomotor task, as well as auditory and somatosensory stimulations. Detailed steps of the data analysis pipeline are further presented for performing EMSI as well as individual ESI and MSI using equivalent current dipole (ECD) and dynamic statistical parametric mapping (dSPM).

Introduction

Epilepsy is one of the most common and disabling neurological disorders characterized by recurrent and unprovoked seizures that can be either focal or generalized in nature. Despite the availability of several effective pharmacologic therapies (e.g., antiseizure medications [ASMs]), about 20-30% of these patients are unable to control their seizures and suffer from drug-resistant epilepsy (DRE)[1]. For these patients, epilepsy surgery is the most effective treatment to eliminate seizures; a successful surgery can be achieved through the complete resection (or ablation/disconnection) of the epileptogenic zone (EZ), defined as the minimal area indispensable for the generation of seizures[2]. Accurate delineation and resection (or ablation/disconnection) of the EZ while preserving the eloquent cortex are crucial factors in ensuring seizure freedom. To establish surgical candidacy, several noninvasive diagnostic tools are used by a multidisciplinary team to define different cortical areas (i.e., irritative zone, seizure onset zone [SOZ], functional deficit zone, and epileptogenic lesion), which serve as indirect approximators of the EZ[3]. Extra-operative monitoring with intracranial EEG (iEEG) is required when none of these methods unequivocally identify the EZ. The role of iEEG is to define precisely the EZ by localizing the SOZ (i.e., the brain area where clinical seizures generate) and map eloquent brain areas. Yet, it presents serious limitations due to its invasiveness[4,5,6], it offers limited spatial coverage, and it needs a clear presurgical localization hypothesis[7]. As a result, the actual focus and extent of the SOZ may be missed, leading to unsuccessful surgery. Also, its interpretation requires the recording of multiple stereotyped clinical seizures during several days of hospitalization, which increases the chances of complications (e.g., infection and/or bleeding)[5]. Hence, there is an unmet need to develop reliable and noninvasive localization methods that can provide clinically useful information and overall improve the presurgical evaluation of children with DRE.

Over the last decades, electric and magnetic source imaging (ESI and MSI) have been increasingly utilized in the presurgical evaluation of patients with DRE for the delineation of epileptogenic as well as functional brain areas. Particularly, ESI and MSI allow the reconstruction of neural sources from noninvasive recordings, such as high-density EEG (HD-EEG) and magnetoencephalography (MEG), to help guide surgical planning or iEEG electrode placement. ESI and MSI can be applied for localizing either interictal epileptiform discharges (IEDs), such as spikes and sharp waves, or ictal (seizure) activity. It may further be used for the localization of different functional brain areas involved in sensory, motor, auditory, and cognitive functions. The reconstruction of electrophysiological events, such as IEDs and seizures, allows the identification of the irritative zone (i.e., the brain area where IEDs originate) and the SOZ, respectively, which are considered a valid surrogate for the EZ localization. The localization of the eloquent cortex (i.e., the brain areas indispensable for defined cortical functions)[3] allows instead to map the location and extent of eloquent areas with respect to the planned resection and, therefore, reduce in advance potential functional deficits that may be expected from epilepsy surgery[8,9,10,11]. Several studies investigated the clinical utility of ESI and/or MSI in the presurgical evaluation of epilepsy, and they showed promising findings in the delineation of the EZ[12,13,14,15,16,17,18,19]. For example, Mouthaan et al.[14] performed an extensive meta-analysis using noninvasive data of 11 prospective and retrospective

epilepsy studies and reported that these source localization techniques can overall identify the EZ with high sensitivity (82%) and low specificity (53%). Other studies also showed that MSI and ESI can correctly localize the epileptic focus within the resected area in epileptic patients having a normal magnetic resonance imaging (MRI)[19,20,21]. These localization results are particularly important for those patients who are ineligible for epilepsy surgery due to inconclusive clinical or imaging findings. In summary, ESI and MSI can contribute significantly to the presurgical mapping of epileptogenic as well as functional brain areas in patients with DRE.

Despite these encouraging findings, such techniques are currently performed in only a few tertiary epilepsy centers on a regular basis and are often underutilized in pediatric populations. Moreover, HD-EEG and MEG are rarely recorded simultaneously, although they provide both confirmatory and complementary information. MEG is sensitive to detect superficial sources with tangential orientation but is blind to radially oriented sources located at the gyri or deeper areas of the brain[22,23,24,25,26]. Furthermore, MEG provides better spatial resolution (millimeters) compared to EEG[16,22,25]. Unlike EEG signals, MEG signals are reference-free and are essentially unaffected by different conductivities of brain tissues (i.e., meninges, cerebrospinal fluid, skull, and scalp)[25,27] providing undistorted measurements of the magnetic fields produced by the brain. On the other hand, EEG can detect sources of all orientations, but it offers lower spatial resolution than MEG and is more susceptible to artifacts[26,28]. Due to these complementary sensitivities to source orientation and depth, approximately 30% of the epileptiform activity (e.g., IEDs) can only be recorded on MEG but not on EEG, and *vice versa*[26,29,30,31,32]. Contrary to EEG, which allows prolonged recordings, capturing clinical seizures with MEG is challenging due to the restricted recording time that is usually insufficient to record ictal events in most patients. Furthermore, artifacts caused by seizure-related head movements can often interfere with the quality of MEG recordings[29,33,34,35]. On the other hand, MEG recordings are faster and easier compared to EEG, especially in children since there is no need to attach sensors over the children's head[35].

Advances in hardware have made it possible to record simultaneously MEG and HD-EEG data with a high number of sensors (over 550 sensors) covering the whole head. Moreover, modern developments in EEG technologies have minimized the preparation time for HD-EEG to less than a quarter of an hour[36]. This is particularly important for pediatric populations with challenging behaviors who are unable to stay still for prolonged periods. Furthermore, advancements in software technologies have allowed the combination of ESI and MSI into a single solution, namely electromagnetic source imaging (EMSI), performed on simultaneous HD-EEG and MEG recordings. Several theoretical and empirical studies reported higher source localization accuracy with EMSI than either modality alone[13,30,31,37,38,39,40,41]. Using different source localization approaches to reconstruct the activity in response to sensory stimuli, Sharon et al.[37] found that EMSI had consistently better localization results than either ESI or MSI alone compared to functional MRI (fMRI), which serves as noninvasive benchmark of precise localization accuracy. The authors suggested that this improved localization is due to the increased number of sensors for solving the inverse solution and the different sensitivity patterns of the two imaging modalities[37]. Similarly, Yoshinaga et al.[31] performed dipole analysis on simultaneous EEG and MEG data of patients with intractable localization-related epilepsy

and showed that EMSI provided information that would be not obtainable by using only one modality alone and led to successful localization for epilepsy surgery in one of the patients analyzed. In a prospective blinded study, Duez et al.[13] showed that EMSI achieved a significantly higher odds ratio (i.e., probability of becoming seizure-free) compared to ESI and MSI, a localization accuracy ≥52%, and a concordance ≥53% and ≥36% with the irritative and SOZ, respectively. A more recent study from our group[42] has shown that EMSI provided superior localization estimates and better outcome prediction performance than either ESI or MSI alone, with localization errors from resection and SOZ of ~8 mm and ~15 mm, respectively. Despite these promising findings, there is a lack of studies that provide the methodological framework regarding EMSI in children with DRE.

This study illustrates the experimental setup for performing simultaneous MEG and HD-EEG recordings as well as the methodological framework for analyzing these data aiming to localize the irritative zone, SOZ, and eloquent brain areas in children with DRE. More specifically, the experimental setups are presented for (i) recording and localizing interictal and ictal epileptiform activity during sleep and (ii) recording visual-, motor-, auditory-, and somatosensory-evoked responses and mapping relevant eloquent brain areas (i.e., visual, motor, auditory, and somatosensory) during a visuomotor task, as well as auditory and somatosensory stimulations. Detailed steps of the data analysis pipeline are further presented for performing EMSI as well as individual ESI and MSI using equivalent current dipole (ECD) and dynamic statistical parametric mapping (dSPM).

Protocol

The experimental procedures applied here have been approved by the North Texas Regional Institutional Review Board (2019-166; Principal Investigator: Christos Papadelis). The following section will describe the experimental protocol for the noninvasive source localization of IEDs, ictal onsets, and event-evoked responses (i.e., visual, motor, auditory, and somatosensory) using simultaneous MEG and HD-EEG recordings followed in our laboratory. The International Federation of Clinical Neurophysiology[43] and the American Clinical MEG Society[44] have provided "minimum standards" for the routine clinical recording and analysis of spontaneous MEG and EEG data. Procedures for HD-EEG recordings described here apply only to sponge-based EEG electrode systems. The overall preparation process for each subject is about 2-3 h, comprising the actual recordings of ~1.5 h.

1. MEG system's preparation

1. Before the subject's arrival, perform an empty-room MEG recording of a few minutes to capture the background noise levels and magnetic artifacts and check that all MEG sensors are working properly.
2. Using the MEG sensors tuning program, ensure that the average white noise value of all MEG sensors is between 2 and 5 fT/√Hz (fT/cm√Hz for gradiometers).

2. Subject's preparation

1. Ensure that the subject is comfortable with the environment. In the case of young children, allow them to explore the recording room (including the magnetically shielded room [MSR]) and see the testing equipment that will be used for data acquisition.

1. Screen and provide the subject instructions using the screening consent form. If needed, explain the procedure to young children using special words, toys, and games developed for each age group. Ask the subject (or the subject's parents) if he/she had a seizure within the last ~2 h prior to the visit.

   NOTE: The screening consent form includes a description of the test, as well as its safety, why the testing is performed, and an overall description of the study.

2. Remove any metallic and/or magnetic materials from the subject and provide the subject with appropriate hospital-issued clothes (e.g., hospital gowns, scrubs). In addition, ask the subject to remove his/her shoes to prevent magnetic dust from entering the MSR. If other ferromagnetic elements, such as dental works or implanted medical devices, cannot be removed, use a degausser (i.e., demagnetizer) to remove residual magnetic artifacts that can cause either interferences or high noise levels during MEG recordings. After making sure that all sources of magnetic noise have been removed, ask the subject to sit and get comfortable on a wooden chair where the next measurement procedures will be applied.

   NOTE: The degausser must not be applied directly to any implanted electronic devices (e.g., pacemakers, neuromodulation devices).

3. Measure the subject's head circumference to select the appropriate EEG net size (usually 32-34 cm up to 58-61 cm). Using the centimeter side of the measuring tape, measure the head circumference by holding the tape from the subject's nasion to ~1 cm above the inion and then back to the nasion.

   NOTE: The nasion is the craniometric point between the eyes, whereas the inion is the tip of the external occipital protuberance.

   1. Select the correct net size that fits the subject's head circumference and soak it for at least 5 min (10 min maximum) into a liquid mixed solution composed of 1 qt of warm tap water, 1 tbsp of electrolytes (i.e., Potassium Chloride), and 1 tbsp of baby shampoo. During this soaking process, ensure that the net is turned inside out with the sponges facing out and the clasps fully loosened to fully immerse the sensors inside the plastic bucket containing the solution.

      NOTE: To ensure that the net's amplifier does not come near the solution and always remains dry, wrap a towel around the plug of the selected net and, if preferable, place it on a chair or support close to the sink where the plastic bucket is.

4. Place five magnetic coils served as head position indicator (HPI) coils at known locations directly on the scalp of the subject using micropore paper tape: one on each side of the forehead near the hairline, one on each mastoid bone, and one on the top of the head.

   NOTE: The HPI coils define the position of the head relative to the superconducting quantum interference devices (SQUIDs) placed inside the MEG system by emitting known magnetic fields that can be localized during the scan. The number of HPI coils depends on the MEG system, but it usually ranges from 3-5 HPI coils.

5. Place additional electrodes using tape to measure heart rate (electrocardiography, ECG), eye movements or blinks (electrooculography, EOG), and muscle activity (electromyography, EMG); the placement of these electrodes also allows the monitoring of the subject's health state.

1. Place two ECG electrodes on the right and left side of the chest below the collarbones, respectively, to record the subject's heartbeat, and two EOG electrodes on the upper and lower side of the right eye, respectively, to record his/her vertical eye movements or blinks.
    1. To measure the muscle activity during the visuomotor task, additionally, wipe the subject's fingers with alcohol pads for better adhesion of the tape on the skin and tape a total of two pairs of non-disposable cup electrodes on each hand: one on the first dorsal interosseous (FDI) and one on the abductor pollicis brevis (APB).
    2. Before taping all these electrodes, place the conductive paste inside the electrode cup until it is slightly overfilled to reduce skin impedance and ensure an optimal blend of adhesiveness and conductivity.
2. For tactile stimulation, attach thin elastic membranes directly to the distal, volar parts of three digits (i.e., thumb [D1], middle finger [D3], and pinky [D5]) of both hands. Inflate the membranes with compressed air pulses through rigid plastic tubes using an air puff stimulation device. Release the compressed air pulses with an inter-stimulus interval of 1.5 ± 0.5 s following a pseudorandom order. Adjust the pressure of the tactile stimulator to 50 psi.

6. While the subject still sits on the wooden chair distant from any metallic object, determine the three-dimensional (3D) positions of the fiducial anatomical landmarks, five HPI coils, and other head shape points using a digitizer. During this head digitization process, ask the subject to sit comfortably, look straight ahead, and remain virtually motionless since small movements may affect the localization accuracy.
    1. Place the reference receiver through the plastic goggles (i.e., eyeglasses with the reference cube attached on one side) on the subject's head and adjust the clasps to ensure a fixed reference frame to the subject that must stay relatively still during the entire measurement.
    2. Through the primary stylus receiver, locate the fiducial anatomical landmarks (i.e., nasion and left/right preauricular points) and the HPI coils' position, and uniformly sample additional scalp points (at least 100, preferably close to ~500) to enhance a high-quality reconstruction of the head surface.
        NOTE: The fiducial anatomical landmarks define the subject coordinate system. The digitizer generates the coordinates of a sensor in the 3D space using one transmitter (typically mounted behind the subject on the back of the wooden chair) and two receivers (i.e., the stylus and reference receivers).
    3. After the digitization is completed, place the stylus receiver ~15 cm away from the subject and transmitter and digitize a random point to finish the digitization process.
        NOTE: This final step of the digitization process may differ from other commercial products.
7. Before applying the EEG net, ask the subject to sit on a chair close to the EEG amplifier and place towels on his/her chest and shoulders to absorb eventual drips due to the net's application. Remove the EEG net from the plastic bucket, turn it with the sponges facing the inside, and gently wrap it around a towel to absorb the mixed solution in excess.

1. With the subject sitting on the chair and instructed to keep his/her eyes closed during this step, put both hands inside the net and spread it using fingers, and finally place it on the subject's head.
2. Without moving the positions of the HPI coils, adjust the stretched net on the subject's head using fingers to ensure that the reference and nasion channels are correctly positioned at the center of the scalp and between the subject's eyes, respectively, and finally fasten the chin strap once the net is in the correct position.

8. Using an EEG impedance meter, ensure that all scalp-electrode impedances are in the 0-50 kΩ range (values <5 kΩ are recommended) to prevent any signal distortions. To reduce the scalp-electrode impedances, check that each electrode has good mechanical and electrical contact with the scalp by using either a wooden cotton swab to remove the subject's hairs between the electrode and the scalp or a disposable plastic pipette to transfer more conductive mixed solution into the sponges of the electrodes if needed.
    1. Once all the impedances are ideally up to 50 kΩ, disconnect the amplifier and prepare the subject for the EEG electrode digitization.
       NOTE: Perform the EEG electrode digitization outside the MSR and ensure enough room around the subject to manage the scanning process.
9. Determine the 3D positions of the EEG electrodes using a handheld optical scanner. During this process, ask the subject to sit comfortably and look straight ahead unless instructed otherwise.
    1. Firstly, open the optical scanner software, select the sensor template that matches the EEG sensor layout used during the recordings, and then initiate the scanning process.
    2. During the scanning, hold the scanner at a certain distance from the EEG net (usually ~45 cm), with its scanning apertures perpendicular to the surface of the sensors, and slowly move it around the subject's head following arched swaths from the top (center of the head) to the bottom (last sensors row along the neck) to record the physical locations of all sensors.
       NOTE: The optical scanner digitizes the EEG electrode locations on the subject's head and transforms them as a 3D coordinate file; it is usually characterized by two optical sensors that emit infrared (IR) light sources. Each scanned location usually appears on a 3D sensor cloud. The 3D sensor cloud provides feedback for the scanning, probing, and alignment of the sensor positions, whereas the 2D sensor map provides feedback for the labeling of these sensor positions. The scanning process of the EEG electrode positions requires a total of 5-10 min, including the probing of the fiducial points. However, the scanning time may sometimes depend on the performance of the optical scanner in detecting the electrode positions.
10. Once all the EEG electrodes have been scanned (at least 95%), probe the fiducial points (i.e., nasion and left/right preauricular points) and four alignment sensors (i.e., front, left, and right align nodes, and REF node) using the wireless optical probe to align the 3D sensors cloud to the selected sensor template.
    NOTE: The alignment sensors are numbered based on the EEG sensor net configuration.
    1. To probe the fiducial points, place the optical probe's tip on the subject's skin at the center of the fiducial

point of interest by ensuring that the scanner's scanning apertures point at the probe's reflective disks. Similarly, place the optical probe's tip at the center of the alignment sensor of interest to probe the alignment sensors.

11. Once all the sensors have been scanned and probed, review their positions and labels on the 3D sensor cloud and 2D sensor map with respect to the actual EEG net to check and eventually correct possible errors; if no errors occurred during the scanning process, export the 3D coordinate .txt file and convert it into the preferable format.

    NOTE: The 3D electrode coordinates are usually stored in .txt format and can be converted via optical scanner software in several formats (e.g., .xml, .sfp, .elp, or .nsi).

12. After the EEG electrode digitization process (steps 2.9-2.11) is completed, prepare the subject to be transferred inside the MSR for performing resting/ sleeping data (step 2.13), visuomotor task (step 2.14), auditory stimulation (step 2.15), and somatosensory stimulation (step 2.16).

13. For the resting/sleeping data, set the gantry of the MEG system to the supine position (**Figure 1A**) and arrange the nonmagnetic and compatible bed so that the removable headrest is aligned with the helmet-shaped opening at the bottom of the dewar. After adjusting the bed to the correct position, set the brake valve of the bed to the off locked position. Place a sheet or blanket over the bed and a small foam pad pillow on the removable headrest for head fixation and comfort during the recording.

    NOTE: The dewar is a cryogenic storage container filled with liquid helium in which sensor arrays are spatially arranged at the bottom via a helmet-shaped opening designed to surround the subject's head. The helmet fits up to 59-61 cm head circumference. The gantry is the mechanical system supporting the dewar that allows modifying its elevation and angle based on the measurement position (i.e., seated or supine).

    1. Transfer the subject inside the MSR and help him/ her sit on the edge of the bed and lie down on it. Place several blankets on the subject's body to keep him/her warm during the recording by ensuring that the electrodes' cables are easily accessible, and lightly fasten the safety belts (or pull up the railings if present), explaining to the subject that this step is to prevent him/her from rolling out of the bed while sleeping. If needed, place an additional rolled towel under the neck to provide support for the subject's neck and shoulders.
    2. Unlock the brake valve of the bed to gently move the subject's head, which is placed on the removable headrest under the helmet-shaped opening of the dewar until it touches the inside of the helmet. To increase the signal-to-noise ratio (SNR), bring the subject's head as close to the helmet as possible.
    3. Plug the HPI coils, ECG, and EOG electrodes on the corresponding panels of the MEG system, connect the EEG net to the amplifier unit inside the MSR, and check the measurements of the head's coordinates from the acquisition workstation outside the MSR to assess whether the subject's head is properly positioned under the dewar.
    4. With the subject's consent, reduce the intensity of the light inside the MSR to help stimulate relaxation and sleep. When the subject feels relaxed and comfortable, instruct the subject to rest with his/her

eyes closed or sleep during the recording. Reassure the subject that he/she will be observed on the monitor outside the MSR via the radiofrequency-shielded color camera mounted on the wall of the MSR for the entire recording.

14. For the visuomotor task, set the gantry of the MEG system to the upright position (**Figure 1B**) and arrange the MEG chair so that the subject's head is under the gantry, close to the helmet-shaped opening at the bottom of the dewar. After adjusting the chair to the correct position, set the brake valve of the chair to the off-locked position ("0").

    1. Transfer the subject inside the MSR. Help him/her to sit on the nonmagnetic and compatible chair and find a comfortable and relaxed position. Place several blankets on the subject's body to keep him/her warm during the recording by ensuring that the electrodes' cables are easily accessible, and place the removable table so that the subject can put his/her hands on it during the task. If needed, place a towel under the subject's knees to help maintain the seated position, and do not slide down.

        NOTE: Since the subject may relax during the visuomotor task and, therefore, assume a lower position than the initial one, carefully lift the chair at the end of each task session via the elevation pedal (if present) or place towels or blankets on the chair so that the subject's head touches the inside of the helmet again. If needed, place additional towels or blankets behind the subject's head not only for better comfort but also to help the subject keep the head as straight as possible. Visuomotor stimulation can be performed alternatively in a supine position to avoid moving the dewar in the middle of a recording session.

    2. Once the subject is in the right position, plug the HPI coils, ECG, EOG, FDI, and APB electrodes on the right panel of the MEG machine, connect the EEG net to the amplifier unit inside the MSR, and raise the chair through the elevation pedal (if present) with small movements or place additional towels or blankets on the chair until the subject's head lightly touches the inside of the helmet (check the measurements of the head's coordinates from the acquisition workstation outside the MSR).

    3. Place the projection screen, in which the visual stimuli will be projected via a projector mirror system positioned outside the MSR, in front of the subject (**Figure 1B**), and explain the visuomotor task to perform during the recording. Particularly, instruct the subject to tap his/her index finger on the table only when the visual stimulus (e.g., an image) appears on the screen, respectively, for the right and left hand. Make sure that the subject understands the task or feels comfortable performing it alone; if needed, practice the task together with the subject several times to help him/her get familiar with it.

        NOTE: If a visuomotor stimulation session is performed in a supine position, a mirror is placed at a distance above the subject's face to reflect the visual stimuli from the projector.

    4. Before closing the door of the MSR, ask the subject if he/she feels comfortable being alone inside the room; in case he/she does not, either one person from the team or his/her parents will remain inside the MSR during the recording sessions. Moreover,

reassure the subject that he/she will be observed on the monitor outside the MSR for the entire recording.

15. For the auditory stimulation, use the setup described in step 2.14 with the projection screen in front of the seated subject. Help the subject to wear the headphones (or earphones) through which the sound triggers (e.g., modulated chirp sounds) are delivered.

    1. Instruct the subject to fixate the stimuli (e.g., green point on a black background) projected on the screen while listening to the sound triggers. If needed, perform a training session to help the subject better understand the procedure. Before closing the door of the MSR, repeat the safety procedures as previously described.

16. For the somatosensory stimulation, use the setup described in step 2.14. Ask the subject what video (or movie) he/she wants to watch on the projector screen in front of him/her.

    1. Instruct the subject to relax with eyes open, watch the selected video, stay as still as possible, and ignore the tactile stimuli delivered to his fingers during the recording. Explain to the subject that he/she will feel gentle taps on the skin at the tip of the fingers, respectively, for each hand. If the subject feels uncomfortable, perform a training session to reassure him/her.

       NOTE: Eye fixation on a visual target is a well-established technique to minimize biological artifacts that can affect the quality of the recording and distract the subject from the tactile stimuli delivered during the data acquisition.

3. Data acquisition

NOTE: The acquisition of simultaneous MEG and EEG data is performed in the MEG facility at Cook Children's Medical Center (CCMC). More details about the clinical use of MEG on pediatric children with epilepsy can be found elsewhere[8,27,45].

1. Record MEG signals using the whole-head MEG system (sensor coverage: 1,220 cm^2) characterized by 306 channels grouped in 102 identical triple-sensor elements with one magnetometer and two orthogonal planar gradiometers. Set a sampling frequency of at least 1 kHz.

   NOTE: Single-coil magnetometers measure the component of the magnetic field perpendicular to the MEG helmet surface. Planar gradiometers consist of a "figure-of-eight" coil configuration characterized by pairs of magnetometers placed at a small distance between each other and measure the difference in the magnetic field between their locations (i.e., the difference between the two loops of "eight"), also named spatial gradient. Compared to magnetometers, planar gradiometers are less sensitive to deep brain sources but more robust in detecting superficial sources by suppressing environmental noise. These 306 channels are immersed and cooled down in liquid helium at -296 °C (4.2 K) to become superconductors.

2. Record EEG signals simultaneously using the nonmagnetic 256-channel EEG net with Ag/AgCl electrode sensors evenly spaced over the scalp, cheeks, and back of the neck. Set a sampling frequency of at least 1 kHz.

3. Close the door of the MSR to begin recording. Through the voice intercom system, communicate with the

subject, checking if he/she feels comfortable being alone inside the MSR. Constantly monitor the subject on video and, in an emergency, immediately enter the MSR.

NOTE: In case he/she does not feel comfortable or the massive MSR door is intimidating him/her, either one person from the team or his/her parents can remain inside the MSR during the recording sessions seated on a wooden chair close to the subject; ensure that all metallic objects are removed before entering the room.

4. Before each recording, instruct the subject through the voice intercom system to keep his/her position still for ~30 s before starting the task. For the visuomotor task, additionally communicate via the intercom which index finger (either right or left) he/she will use for the first recording session.

    1. During this period in which the subject stays still, press the measure button from the HPI measurement dialog on the MEG data-acquisition system to measure the magnetic field generated by current fed into the HPI coils and determine the head measurement positions with respect to the MEG sensor array; therefore, confirm that the subject is well positioned (**head |z-coordinate| < 75 mm**) and write down the 3D measurements for each session.

    2. If there is still space between the subject's head and the helmet, either re-enter inside the MSR and adjust the height of the chair via the elevation pedal (if present), place towels or blankets on the chair, or instruct the subject via the intercom on how to shift the head in a closer position to the helmet (if the subject is seated), and finally check the head measurement positions again. In case of resting/ sleeping recordings, re-enter the MSR and bring the bed closer to the helmet, reducing the head-helmet spatial gap.

5. Once the subject is well positioned with respect to the MEG helmet and ready to start, begin the first recording session (duration ~10 min) by following a precise order (see step 3.5.1) for accurate MEG and EEG synchronization (see step 3.12).

    NOTE: To ensure high-quality recordings, the first recording session is critical to capture artifacts present in the data due to movements of the subject or caused by the external environment. If needed, re-enter inside the MSR to adjust eventual channel connections or the subject's position on the MEG chair. It is recommended to take notes of any unusual artifacts or events during the recordings that can be reviewed afterward if needed.

    1. Press the recording button on the EEG data-acquisition software to begin the EEG recording. Press the recording button on the MEG data-acquisition software to begin the MEG recording. Finally, press the start button from the software of the stimulation computer to either display visual stimuli or deliver auditory stimuli.

        NOTE: The stimulation computer running the visual (or auditory) stimulus software is connected to the projector mirror system outside the MSR, which can be turned on or off depending on the type of recording performed. During resting/sleeping recordings, the system is turned off since the subject is either resting or sleeping, but running the visual stimulus software on the stimulation computer helps timing each recording session. During the visuomotor task, as well as during the auditory and somatosensory stimulations, the system is turned on by allowing the subject to observe the stimuli

or a video projected on the screen placed in front of him/her while the software is running. For this study, it was selected a total of (i) 107 stimuli (i.e., 85 images overlaid on a checkerboard background and 22 checkerboard backgrounds) with a ~4 s interval between each stimulus for the visuomotor task; (ii) 200 modulated chirp sounds with an inter-stimulus interval of 3 s for the auditory stimulation; and (iii) 200 tactile stimuli for each finger (i.e., D1, D3, and D5) following a semi-random sequence with an inter-stimulus interval of ~1.5 s for the somatosensory stimulation.

6. To stop the recordings, press the stop button on the MEG data-acquisition software and then the stop button on the EEG data-acquisition software. At the end of each recording session, communicate with the subject via the intercom to reassure him/her and if no channel connections or position adjustments inside the MSR are needed, proceed with the next session.
    1. For the visuomotor task, select different visual stimuli for each session to keep the subject motivated and entertained during the recording.
7. For either visuomotor or resting/sleeping data, record a total of ~1 h simultaneous MEG and EEG recording, characterized by 5-6 sessions. However, the number of sessions may vary for each subject. Further, record a total of ~20 min (1-2 sessions of ~10 min each) and ~14 min (1-2 sessions of ~7 min each) of simultaneous MEG and EEG recording for the auditory and somatosensory stimulation data, respectively.

    NOTE: In this study, the MEG and EEG data are automatically stored at the end of the recordings as .fif and .mff formats, respectively, in the IT storage system of CCMC.
8. When the recording ends, enter the MSR to help the subject stand up from either the chair or bed and ask him/her to sit on a chair outside the MSR to remove both the EEG net and electrodes.
    1. Instruct the subject to close his/her eyes until told otherwise and help him/her to remove the EEG net by fully loosening the chin straps and gently pulling out the net using two hands (from the forehead towards the back of the subject's head) until it is completely peeled away. During this step, ensure not to pull the subject's hair while removing the net. Additionally, help the subject to gently remove the remaining electrodes (i.e., ECG, EOG, and EMG in case of visuomotor task) previously taped on his/her skin.
9. After the EEG net and electrodes are removed, inform the subject (and his/her parents) that all the procedures are finally completed.
10. After the subject leaves the room, carefully clean the optical scanner (as described in the user manual) and store it inside its protective case.
    1. Clean and disinfect the surfaces of any equipment used during the recordings (e.g., chairs, beds, desks) with either hospital-approved hydrogen peroxide wipes or disinfecting spray and paper towels, put the used blankets and towels inside the container provided by the hospital, and throw away any piece of used tape.
    2. Store the measurement tools inside the storage cabinet and clean the inside of the electrode cups filled with conductive paste using wooden cotton swabs under running tap water.

3. To rinse the EEG net, fill the plastic bucket in the sink with clean, warm tap water and repeat the following steps for a total of four times.
    1. Submerge the EEG net in the water and gently agitate the EEG net for 10-20 s (or dip it inside and outside the bucket ~25 times).
    2. Drain the water from the bucket, and refill the bucket with clean and warm tap water.
4. To disinfect the EEG net, fill the plastic bucket in the sink with the disinfecting solution composed of 2 qt of lukewarm tap water and 1 tbsp of disinfectant and soak the EEG net inside it for 10 min. Rinse the bucket from the disinfecting solution and follow the rinse-and-drain process three times to remove any residual solution from the EEG net.
5. For either the rinsing or disinfecting process, remove the immersed EEG net from the bucket, dry it by removing the excess water with the help of a clean, dry towel, and store it by hanging it close to the sink.

11. To suppress internal and external magnetic interferences and measurement/movement artifacts from the MEG data, apply the temporal extension of the signal space separation (tSSS) method to the raw-data MEG .fif file.
    NOTE: The spatiotemporal Maxwell filtering (tSSS) is ideal for suppressing sources of interference located inside or very close to the MEG sensor array, namely internal interference.
12. When performing simultaneous MEG and EEG recordings, spatially align the coordinate systems of the two acquisition devices with respect to the anatomical landmarks on the subject's head (**Figure 2A**) and correct the linear clock drift between signals that occurs due to the possible different sampling rates (**Figure 2B**).

NOTE: During the recordings, both MEG and EEG signals can be also affected by slow shifts over time due to possible delays in pressing the **Start** and **End** buttons and to an internal clock drift that occurs when the triggers are sent to the MEG and EEG data-acquisition software. To ensure precise synchronization between these signals, an in-house code was developed in *Python* that uses the trigger events sent on both systems during the data acquisition as common trigger signal. The code includes three functions available in the *MNE-Python* software library: two functions that read the MEG and EEG signals and one function that extracts information of the trigger events from the signals, such as channel names and timestamps (i.e., date and time of the event occurrence). Differences in time between the occurrence of trigger events in each signal (i.e., delta) define the linear clock drift over time (**Figure 2B**). A detailed description of the developed code is provided in the next steps (see 3.12.1-3.12.4).

1. Use the difference between the first trigger event occurring on each signal as offset value (i.e., portion to be trimmed from one of the two signals) to align the recordings.
    NOTE: The **mne.io.read_raw_fif** and **mne.io.read_raw_egi** functions convert the MEG and EEG recordings in a 2D array format, whereas the **mne.find_events** function extracts event information from the raw signals.
2. Once these first triggers are aligned, compute the Pearson's correlation coefficient to assess the degree of correlation between the signals; *p*-values $< 1 \times 10^{-6}$ are recommended to ensure a perfect alignment.

NOTE: The **pearsonr** function from the **scipy** library estimates the Pearson's correlation coefficient between MEG and EEG signals and the *p*-value of this correlation.

3. To validate this correlation accuracy, estimate the drift rate between the two signals by performing a first-degree polynomial fit and use the resulted extent of disparity represented by the coefficient of the polynomial function to resample the signals on the x-axis of the polynomial fitting (**Figure 2B**).

   NOTE: The **polyfit** function from the **numpy** library fits the MEG and EEG signals within a polynomial function; this function returns a coefficient that represents the extent of disparity between the two signals. The **mne.resample** function resamples the MEG and EEG signals according to the coefficient of the polynomial function.

4. After the resampling is complete, compare the timestamps of the last trigger event occurring on each signal and remove those time windows that are not common in both MEG and EEG signals. Finally, merge the synchronized MEG and EEG signals to create a single recording characterized by both MEG and EEG sensors that can be used for further analysis.

   NOTE: The **mne.add_channels** function merges the two signals to create a single recording.

13. At the end of each ~1.5 h recording, use a total of 5-6 (~10 min each), 1-2 (~10 min each), and 1-2 (~7 min each) sessions of synchronized MEG and EEG recordings, respectively for the visuomotor (and resting/sleeping), auditory, and somatosensory stimulation data, for the data analysis.

   NOTE: Ideally, the subject needs to perform right-finger tapping for three visuomotor recordings and left-finger tapping for the remaining three visuomotor recordings.

4. Data analysis

1. Mapping of the irritative zone

   1. Generate the 3D cortical surfaces from the MRI of the subject using the cortical reconstruction process of *FreeSurfer*, which is an open-source neuroimaging tool for processing, analyzing, and visualizing human brain MR images[46].

   2. Import the reconstructed anatomy on *Brainstorm*, which is an open-source application of MATLAB dedicated to MEG and EEG data visualization and processing[47], to visualize the cortical reconstruction results. From *Brainstorm*, set the fiducial points (i.e., nasion, left/right preauricular, anterior/posterior commissure, and interhemispheric) on the imported MRI that define the subject coordinate system.

   3. Import the simultaneous MEG and HD-EEG signal on *Brainstorm* and register the MEG and EEG sensors on the MRI using the MRI registration process to adjust their alignment to the digitized fiducial points. If necessary, project the EEG sensors on the cortical surface.

   4. Open the simultaneous MEG and HD-EEG recording and visually inspect the raw data to remove bad channels. Additionally, apply the signal-space projection (SSP) artifact-correction technique available in *Brainstorm* to reject biological artifacts (e.g., heartbeats, eye blinks) from the recordings.

5. Apply notch (50 or 60 Hz, according to the power-line interference) and band-pass (1-70 Hz) filters to the simultaneous MEG and HD-EEG data.

6. Select portions of data containing interictal activity characterized by frequent IEDs, such as spikes and sharp waves, and having minimal motion artifacts (if possible).

   NOTE: IEDs are transient waveforms characterized by a <70 ms temporal evolution, >50 µV amplitude, and a sharp shape that can be clearly distinguished from the background activity in the 1-70 Hz frequency band[48]. **Figure 3A** represents an example of portions from the simultaneous MEG and HD-EEG signals with frequent IEDs visible on both recordings.

7. Using the standard display setting of 10 s per page, mark the negative peak of each IED that occurs on both MEG and EEG recordings (**Figure 3A**), as well as on each modality alone. Before marking each IED, check the topography field and potential maps for the MEG and EEG, respectively.

   NOTE: Voltage distributions of additional time points during the rising phase of each IED, rather than its peak, must also be checked to account for possible propagating epileptic activity[49]. More details on how to mark interictal spikes events using *Brainstorm* can be found elsewhere (https://neuroimage.usc.edu/brainstorm/Tutorials/Epilepsy).

8. Compute a realistic head model, defined as a three-layer (i.e., scalp, inner skull, and outer skull) geometric model (**Figure 3B**), using the OpenMEEG BEM (symmetric boundary element method) software available in *Brainstorm*. Use the MRI volume as source space (source-point grid with 5 mm spatial resolution).

   NOTE: The OpenMEEG BEM software uses the symmetric boundary element method to compute a realistic forward model characterized by the scalp (i.e., air-scalp interface), outer skull (i.e., scalp-skull interface), and inner skull (skull-brain interface). As an alternative solution, the finite element method (FEM) can be used to solve the forward problem since it allows a realistic subject-specific representation of the head volume conductor. Head tissue conductivity values are often assumed from the literature and may vary depending on the age of the subject[50]. To solve the forward model using the FEM, compute the realistic head model, defined as a three- up to five-layer (i.e., white matter, gray matter, cerebrospinal fluid, skull, and skin) geometric model, using the DUNEuro FEM software available in *Brainstorm*[47,50,51]. More details on the estimation of the forward model using FEM can be found elsewhere (https://neuroimage.usc.edu/brainstorm/Tutorials/Duneuro).

9. Localize the underlying generators of the selected interictal spikes using the unconstrained ECD method on the MEG, EEG, and combined MEG and EEG sensors array separately. To localize these dipole sources, compute the noise covariance from the empty-room MEG recordings or set it as an identity matrix.

   NOTE: Consider performing source localization on averaged IEDs with similar voltage distributions as an alternative approach in case the SNR of IEDs is low[12].

10. Perform the dipole scanning method available in *Brainstorm* at the peak of each IED previously marked to select the most significant source dipoles across the entire brain volume. Select only source dipoles with a goodness of fit >60% and estimate their clusterness defined for each dipole as the number of dipoles located at 15 mm from its center (**Figure 3C**).

    NOTE: More details about the ECD clusterness can be found elsewhere[52].

2. Mapping of the SOZ

    1. Generate the 3D cortical surfaces from the MRI of the subject using the cortical reconstruction process of *FreeSurfer*[46].

    2. Import the reconstructed anatomy on *Brainstorm*[47] to visualize the cortical reconstruction results. Set the fiducial points on the imported MRI that define the subject coordinate system.

    3. Import the simultaneous MEG and HD-EEG signal (containing the ictal event) on *Brainstorm* and register the MEG and EEG sensors on the MRI using the MRI registration process to adjust their alignment to the digitized fiducial points. If necessary, project the EEG sensors on the cortical surface.

        NOTE: If the subject had a seizure during the recordings, review the notes taken during the recording to assess in which session the ictal event was recorded.

    4. Open the simultaneous MEG and HD-EEG recording and visually inspect the raw data to remove bad channels. Apply the SSP artifact-correction technique available in *Brainstorm*[47] to reject biological artifacts (e.g., heartbeats, eye blinks) from the recording.

    5. Apply notch (either 50 or 60 Hz, according to the power-line interference) and band-pass (1-70 Hz) filters to the simultaneous MEG and HD-EEG data.

    6. According to the recording notes, identify the onset of the seizure and its termination (if noted) and mark these events on the signal to identify the correct portion of data containing ictal epileptiform discharges. Examples of a seizure onset are displayed in **Figure 4** for MEG and HD-EEG, respectively.

        NOTE: When a subject has a seizure during the MEG acquisition, medical personnel are required to immediately assist the subject and provide emergency care. Thus, the duration of those data portions with ictal events may be short.

    7. Using the standard display setting of 10 s per page, mark the negative peak of each burst of epileptiform discharges (e.g., repetitive spikes, sharp waves, or spike-wave complexes) occurring during the ictal event on MEG and EEG, as well as on each modality alone. Before each peak marking, check the topography field and potential maps for the MEG and EEG, respectively (**Figure 4A**).

        NOTE: Seizures are classified as generalized or focal depending on where their onset starts. Although dependent on the epilepsy syndrome, a seizure is a phenomenon of at least 10 s characterized by repetitive electrical discharges that may vary in frequency, amplitude, and morphology.

    8. Compute the three-layer (i.e., scalp, inner skull, and outer skull) realistic head model for the MEG and

EEG sensors using the OpenMEEG BEM software available in *Brainstorm*. Use the MRI volume as source space (source-point grid with 5 mm spatial resolution).

NOTE: To solve the forward model using the FEM, compute the realistic head model, defined as a three- up to five-layer (i.e., white matter, gray matter, cerebrospinal fluid, skull, and skin) geometric model, using the DUNEuro FEM software available in *Brainstorm*[47,50,51]. More details on the estimation of the forward model using FEM can be found elsewhere (https://neuroimage.usc.edu/brainstorm/Tutorials/Duneuro).

9. Localize the underlying generators of the selected ictal discharges using the unconstrained ECD method on the MEG, EEG, and combined MEG and EEG sensors array separately. To localize these dipole sources, compute the noise covariance from the empty-room MEG recordings or set it as an identity matrix.

10. Perform the dipole scanning method available in *Brainstorm* at the peak of each ictal waveform previously marked to select the most significant source dipoles across the entire brain volume. Select only source dipoles with a goodness of fit >60% and estimate their clusterness (distance of dipoles from each dipole's center set to 15 mm)[52].

3. Mapping of the eloquent cortex

1. Perform the previously described steps 4.2.1-4.2.3 using the signals recorded during the visuomotor task, as well as during the auditory and somatosensory stimulations.

2. Open the simultaneous MEG and HD-EEG recordings and visually inspect the raw data to remove bad channels. Separately, for each session, apply the SSP artifact-correction technique available in *Brainstorm*[47] to reject biological artifacts (e.g., heartbeats, eye blinks) from the recordings. Additionally, discard or mark as "Bad interval" all those data segments contaminated by artifacts that cannot be used for further analysis.

3. Apply notch (either 50 or 60 Hz, according to the power-line interference) and band-pass (1-100 Hz) filters to the simultaneous MEG and HD-EEG data.

4. For mapping the motor cortex, open the EMG signals recorded from the FDI and APB electrodes and manually mark the tapping event performed by the subject, separately for the right and left hand, by selecting the first peak of muscle activation different from the baseline on the FDI pair-electrode. Perform this step separately for each session using *Brainstorm*[47].

NOTE: Use the **Filter** tab for visualization only on *Brainstorm* and select frequency ranges (e.g., high-pass: 30 Hz; low-pass: 300 Hz; notch: 60 Hz) that can help to correctly mark the peaks of the EMG activity while tapping. The name of the events needs to be the same across sessions; for example, events when the subject performed the right-finger (or left-finger) tapping can be named as "Tap_right" (or "Tap_left"). This step allows us to perform a unique analysis on the same type of event that occurred across all sessions.

5. From each session, import the events occurring on artifact-free segments by selecting the following

parameters: visual stimuli: [-200; +500] ms time window, including the baseline of [-200; 0] ms before the stimulus onset; tapping events: [-1500; +1000] ms time window, including the baseline of [-1500; -1000] ms before the visual stimulus onset; modulated chirp sounds: [-500; +1000] ms time window, including the baseline of [-500; 0] ms before the stimulus onset; and tactile stimuli: [-100; +500] ms time window, including the baseline of [-100; 0] ms before the stimulus onset.

6. Once the events of a specific task have been imported from all sessions, apply the average reference montage to increase the SNR on the EEG data and estimate the average across stimuli to obtain the event-evoked fields and potentials. In the case of motor tasks (i.e., tapping) and tactile stimulation, this last step is performed for the right and left hand, respectively.

   NOTE: Panels **A** and **B** of **Figure 5**, **Figure 6**, **Figure 7**, and **Figure 8** show examples of visual-, motor-, auditory-, and somatosensory-evoked responses, respectively, for MEG and EEG and their relative topography field and potential maps. The total number of stimuli for a specific task strictly depends on the number of completed sessions; in the case of motor task, this number also depends on the correctly performed tapping task.

7. For either the visual-, motor-, auditory-, or somatosensory-evoked fields and potentials, compute the three-layer (i.e., scalp, inner skull, and outer skull) realistic head model for the MEG and EEG sensors using the OpenMEEG BEM software available in *Brainstorm*. Use the 3D cortical surface as source space.

   NOTE: To solve the forward model using the FEM, compute the realistic head model, defined as a three- up to five-layer (i.e., white matter, gray matter, cerebrospinal fluid, skull, and skin) geometric model, using the DUNEuro FEM software available in *Brainstorm*[47,50,51]. More details on the estimation of the forward model using FEM can be found elsewhere (https://neuroimage.usc.edu/brainstorm/Tutorials/Duneuro).

8. For each event-evoked fields and potentials, compute the cortical sources on the averaged events using dSPM implemented in the *Brainstorm* toolbox for the MEG, EEG, and combined MEG and EEG sensors array separately. Set the noise covariance matrix using the pre-stimulus baseline period specific for each task (see step 4.3.5).

9. Depending on the task, extract the maximum cortical sources observed at the eloquent brain area involved [primary visual cortex (V1), primary motor cortex (M1), primary auditory cortex (A1), or primary somatosensory cortex (S1)] that can be defined either using an atlas or through the reconstruction of a virtual sensor (i.e., region of interest, ROI) in that location (**Figure 5C**, **Figure 6C**, **Figure 7C**, and **Figure 8C**).

10. Perform the Morlet wavelet time-frequency decomposition on the event-evoked field and potential sources at the eloquent brain area involved (V1, M1, A1, or S1) with a linear scale (frequency range: 1:1:100 Hz).

    NOTE: To estimate evoked oscillations that are time- and phase-locked to the stimulus onset, the MEG/

EEG signal is initially averaged over events and then becomes subject to time-frequency analysis[53,54].

11. Perform standardization of the cortical source maps using the event-related perturbation method available in *Brainstorm* to normalize them with respect to the baseline (see step 4.3.5), separately for each event (**Figure 5D**, **Figure 6D**, **Figure 7D**, and **Figure 8D**).

    NOTE: Standardization of source maps using event-related perturbations is a normalization measure for time-frequency power maps that estimates the deviation from the mean over the baseline in percent. More details of this standardization process can be found elsewhere (https://neuroimage.usc.edu/brainstorm/Tutorials/TimeFrequency#Normalized_time-frequency_maps).

4. Validation

    1. Acquire extra-operative iEEG recording through the implantation of subdural grids and/or depth electrodes. The number, type, and placement of intracranial electrodes are decided by the multidisciplinary epilepsy team based on the clinical hypothesis generated from the summation of information obtained from the noninvasive diagnostic tests of the presurgical evaluation.

        NOTE: As part of the presurgical evaluation, extra-operative iEEG is recorded across several days via a digital EEG system using a 1,024 Hz sampling rate.

    2. Identify the SOZ as defined by an expert epileptologist based on the clinical information available for each subject.

        NOTE: The SOZ is defined as the brain area showing the first unequivocal ictal electrographic discharge, which is different from the background activity that can occur either prior to or concomitant with the clinically defined ictal onset. All channels involved in this ictal electrographic discharge are regarded as SOZ contacts, even if capturing seizures that originate from different brain areas.

    3. During the ictal event recorded on iEEG, mark the peak of each burst of epileptiform discharges occurring at each intracranial electrode and perform source localization on these ictal events using the ECD method as previously described in steps 4.1.7-4.1.10.

    4. Compare the iEEG localization results with respect to the clinically defined SOZ as the gold standard for the source localization results.

Representative Results

Pediatric patients with DRE were recruited from the Epilepsy Clinic at Jane and John Justin Institute for Mind Health, Cook Children's Health Care System (CCHCS). Here, data from three representative patients are presented: (i) a 10-year-old female, (ii) a 13-year-old male, and (iii) a 10-year-old female.

Case 1: A 10-year-old female was admitted with seizures starting at the age of three years. The patient was suffering from daily seizures even after the administration of 8 ASMs. Initial seizures were characterized by eye deviation (unclear side) and behavioral arrest. Later, the patient experienced daily seizures of ~30 s characterized by ictal pouting ("chapeau de gendarme" sign), head deviation to the left, and bilateral tonic arm stiffening (right predominance). Long-term video EEG revealed two clusters of asymmetric

tonic seizures with head deviation to the left, followed by her left arm coming up. Three tonic seizures were also observed while sleeping, with frequent runs of generalized fast polyspikes and slow waves with intermittent eye-opening, upward gaze, and left or right arm elevation. These polyspikes and slow-sleep waves were mostly prominent from the left middle temporal lobe. Brain MRI revealed the following multifocal dysplasias: (i) left parietal lobe (postcentral gyrus) focal cortical dysplasia (FCD) with transmantle sign (type II FCD), (ii) right parietooccipital junction FCD, and (iii) left temporal pole FCD. Positron emission tomography (PET) demonstrated hypometabolism in the left parietal lobe, left temporal lobe, and right parietooccipital junction corresponding to the foci of the signal abnormality (i.e., FCD) on the MRI exam. The patient was diagnosed with intractable epilepsy, with stereotyped semiology of chapeau followed by tonic arm stiffing, suggesting possible mesial frontal or insular/temporal onset. Extensive bilateral stereo-EEG (sEEG) exploration was recommended by targeting the frontal lobe, cingulate, insula, and those regions of dysplasia. During iEEG monitoring, the patient had typical seizures with "chapeau de gendarme" followed by tonic elevation/flexion of the right or left upper extremity characterized by diffuse EEG onset, maximal over the bilateral anterior insula. Multifocal IEDs were mostly observed at the right and left anterior temporal lobe and dorsolateral frontal cortex, including the bilateral insula. ESI performed on iEEG recording confirmed the location of SOZ, which was clinically defined bilaterally at the left and right dorsolateral frontal cortex and anterior insula.

As part of the presurgical evaluation, source localization on the simultaneous MEG and HD-EEG data was performed. MEG and HD-EEG recordings indicated frequent IEDs at both frontotemporal regions. **Figure 3A** shows a representative example of an IED on both MEG and HD-EEG data; topographic field and potential mapping from both modalities indicated a possible underlying source in the right frontotemporal region. ESI indicated a scattered cluster of dipoles covering areas of the right and left frontotemporal and parietal lobes. MSI showed a focal cluster of dipoles in the right frontotemporal lobe, located near the right insula. EMSI indicated focal clusters of dipoles at the bilateral frontotemporal regions, in line with ESI performed on iEEG gold standard, which confirmed the clinical observations (**Figure 3C**). These dipoles estimated through EMSI showed a mean distance from the iEEG-defined SOZ of 9.81 mm (median: 11.18; std: 2.37).

Case 2: A 13-year-old male with intractable epilepsy was admitted with seizures starting at the age of nine years. Seizures started with an aura followed by leftward head/eye deviation with preserved awareness at times and focal clonus of the head to the left, last for ~30 s, and occurred several times per week. None of the ASMs prescribed achieved seizure control. From the long-term video-EEG, we observed right posterior temporal spikes and frequent spike-wave discharges in the right hemisphere involving the middle temporal, frontotemporal, temporoparietal, and centroparietal cortex. The patient had six electroclinical seizures characterized by a behavioral change, head/eye deviation to the left with left arm extension, and sometimes clonic activity of the left arm, and three seizures with secondary bilateral convulsive activity. The maximal onset was at the right middle temporal lobe with an evolution in the right frontotemporal lobe. Brain MRI revealed an extensive malformation of the cortex in the right cerebral hemisphere (perisylvian predominant) and a mild volume loss in the right cerebral hemisphere with ex vacuo dilation of the right lateral ventricle. The patient was diagnosed with intractable epilepsy with onset in the right hemisphere, favoring the

temporal and perisylvian onset in the region of diffuse cortical malformation. Stereo-EEG was performed to delineate the extent of involvement, with electrodes placed in the right temporal, perisylvian, insular, and parietooccipital cortices. Several electroclinical focal onset seizures were captured during the iEEG monitoring with maximal onsets in a wide area of the right frontotemporal lobe. ESI performed on iEEG data localized these seizures in a more focal area comprising both the right temporal (near the right middle temporal gyrus) and perisylvian areas.

As part of the presurgical evaluation, simultaneous MEG and HD-EEG were performed during which the patient experienced two seizures: one while sitting on the wooden chair during the digitization process and one captured during the actual recording with the onset visible on both MEG and HD-EEG (**Figure 4A**). Topography field and potential maps at the ictal onset indicated that the underlying generator of the seizure onset may be at the right middle temporal lobe, as displayed in **Figure 4A**. Source localization on the ictal event presented different findings for ESI and MSI: ESI showed dipoles localized toward the right frontotemporal and centroparietal lobes, whereas MSI showed dipoles with high clusterness mostly at the right temporal lobe (**Figure 4B**), with additional scattered dipoles in the frontotemporal cortex. By combining these solutions, EMSI revealed localization of the ictal onset within the temporal lobe concordant with the ESI on iEEG gold standard (**Figure 4B**). Particularly, EMSI presented localization results with a mean distance from the SOZ defined by the iEEG monitoring of 12.21 mm (median: 13.62; std: 2.37).

Case 3: A 15-year-old female with localization-related idiopathic epilepsy was admitted with seizures starting at the age of 13 years, but possibly at 8-9 in retrospect, when she was diagnosed with tics due to repetitive, stereotyped neck movements. The patient had brief head tilts to the left that sometimes progressed to focal dyscognitive seizure with hypermotor behaviors (i.e., generalized tonic-clonic seizures), as well as nocturnal convulsive seizures. Several ASMs were administered without achieving complete seizure control. During long-term video-EEG monitoring, the patient had focal electroclinical seizures with secondary generalization with onset at the left posterior temporal lobe, numerous brief focal motor seizures with head tilt to the left, and a subtle electrographic seizure with onset at the left centroparietal cortex. Brain MRI revealed no acute intracranial abnormality and a Chiari I malformation. Positron emission tomography-computed tomography (PET-CT) exam of the head resulted negative. Additional testing, such as ictal single-photon emission CT (SPECT), simultaneous MEG and HD-EEG, cervical spine X-ray, magnetic resonance angiography (MRA) of the head and neck, and eventually sEEG exploration of the left hemisphere, was recommended.

As part of the evaluation, the patient participated in simultaneous MEG and HD-EEG recordings for mapping eloquent brain areas, such as the primary visual, motor, auditory, and somatosensory cortices. Initially, the patient performed a visuomotor task, followed by auditory and somatosensory stimulations. The first cortical response to the visual stimulation occurred at ~70 ms after the stimulus onset for both MEG and HD-EEG (**Figure 5A**). **Figure 5B** reports the topography field and potential maps of the cortical locations involved in the visual stimulation for MEG and HD-EEG, respectively. For HD-EEG, a change of polarity in the channels covering the occipital brain areas was observed, whereas a more complex field distribution was found in the same areas for MEG (**Figure 5B**). Source localization using dSPM revealed a focal cortical activity at this time

point within the following brain regions of the Desikan-Killiany atlas: (i) cuneus for MSI; (ii) lateral occipital cortex for ESI; and (iii) cuneus and lateral occipital cortex for EMSI (**Figure 5C**). Time-frequency analysis on visual cortical responses revealed an event-related synchronization (ERS) in the gamma frequency band for MSI (approximate range: 30-50 Hz), ESI (approximate range: 40-50 Hz), and EMSI (approximate range: 30-50 Hz) (**Figure 5D**). For the motor-evoked responses, suppression of the mu-rhythm activity was observed over the contralateral M1 during the movement onset (**Figure 6A**). In **Figure 6B**, we reported the topography field and potential maps of the brain areas activated during the motor task for MEG and HD-EEG, respectively. MEG field maps indicated clear alterations of magnetic influx and outflux in the contralateral central brain areas, which may indicate an underlying focal generator in the contralateral M1 (**Figure 6B**). HD-EEG potential maps showed a focal polarity change in the same areas, with electric potentials perpendicular to the magnetic fields (**Figure 6B**). The peaks of maximal source activation were observed while performing the tapping task at the contralateral precentral gyrus of the Desikan-Killiany atlas for MSI, ESI, and EMSI, respectively, as displayed in **Figure 6C**. Motor-related cortical responses occurring during the anticipation of the upcoming tapping movement showed ERS in beta and gamma bands for MSI (approximate range: 20-30 Hz) and EMSI (approximate range: 20-40 Hz) and gamma band for ESI (approximate range: 30-50 Hz), referred in the literature as *mu rhythm suppression* (**Figure 6D**).[55,56] Auditory-evoked fields and potentials in response to auditory stimulation had a maximum positive peak at ~80 ms and ~120 ms after the stimulus onset delivery for MEG and HD-EEG, respectively (**Figure 7A**). In **Figure 7B**, we reported the topography field and potential maps of the cortical locations involved in the auditory stimulation for MEG and HD-EEG, respectively. In both MEG and HD-EEG, an obvious polarity change with clearly defined negative and positive poles at the sensors covering the left temporal brain areas was observed; these perpendicular magnetic field and electric potential maps may reveal an underlying focal generator in V1 (**Figure 7B**). Performing source localization on the averaged auditory-evoked fields and potentials, maximal cortical activation was observed at the transverse temporal gyrus and posterior portion of the superior temporal gyrus of the Desikan-Killiany atlas for MSI, ESI, and EMSI, respectively (**Figure 7C**). Time-frequency analysis of auditory-evoked responses revealed ERS in the gamma band for MSI (approximate range: 40-60 Hz) and EMSI (approximate range: 35-50 Hz), and beta and gamma frequency bands (approximate range: 25-60 Hz) for ESI (**Figure 7D**). Finally, we observed the first cortical activity in response to the tactile stimulation at ~60 and ~50 ms after the stimulus onset for MEG and HD-EEG, respectively (**Figure 8A**). In **Figure 8B**, we reported the topography field and potential maps of the brain areas activated during the somatosensory stimulation for MEG and HD-EEG, respectively. MEG field maps revealed a clear polarity change with distinct alterations of magnetic flux at sensors covering the contralateral parietal areas, whereas HD-EEG potential maps showed a less obvious change of polarity in the same areas with a stronger positive pole than the negative one. These perpendicular magnetic field and electric potential maps may indicate a focal cortical generator in S1. Using dSPM on the averaged somatosensory-evoked responses, maximal cortical source activity at this time point was observed within the contralateral postcentral gyrus of the Desikan-Killiany atlas for MSI, ESI, and EMSI, respectively (**Figure 8C**). In response to the tactile stimuli, ERS in beta and gamma frequency bands for MSI (approximate range: 15-40 Hz) and EMSI (approximate range: 20-40 Hz), and

gamma frequency band for ESI (approximate range: 30-40 Hz) (**Figure 8D**) were also observed.

Figure 1: Experimental setup for simultaneous MEG and HD-EEG at CCHCS. (**A**) HD-EEG (256 channels) and MEG (306 sensors) systems with the gantry of the MEG set to a supine position (90°, horizontal position) for a resting/sleeping state recording using the nonmagnetic MEG-compatible bed. The technician is preparing the subject (a 9-year-old girl) for the recording while ensuring safety and comfort. (**B**) HD-EEG and MEG systems set for a recording in a seated position using the nonmagnetic MEG-compatible chair. The technician is preparing the subject for the recording while ensuring the correct position of the subject in front of the screen where visual stimuli will be projected during the visuomotor task. Please click here to view a larger version of this figure.

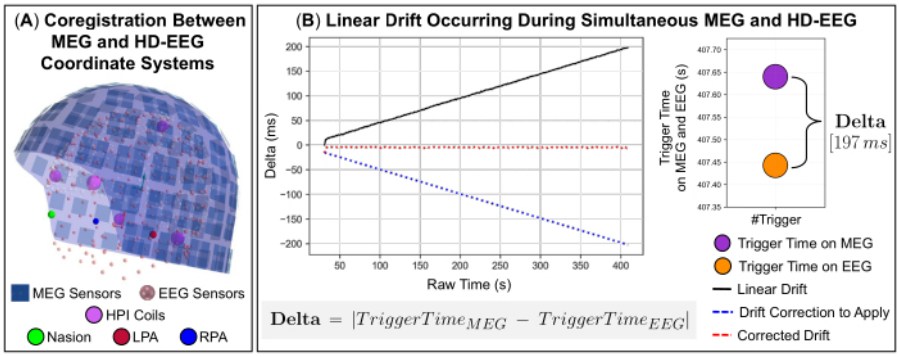

Figure 2: Technical aspects of combining data from simultaneous MEG and HD-EEG recordings using different acquisition systems. (**A**) Spatial alignment (coregistration) of MEG and HD-EEG sensors into the same coordinate system (defined by subject's head coordinates) for a representative subject (a 9-year-old girl). The head coordinates of the subject are represented by the following fiducial points: nasion (green-colored) and left/right preauricular points (red- and blue-colored, respectively). The 306 MEG sensors (blue-colored) - 102 magnetometers and 204 planar gradiometers - and the head position indicator (HPI) coils (magenta-colored) are displayed; aligned into the same coordinate system, the 256 HD-EEG channels are also displayed (pink-colored). (**B**) *Left panel*: Linear drift (i.e., delta, displayed as a black line) of data samples occurring between MEG and HD-EEG systems for a representative subject (a 9-year-old girl). Delta is defined as the absolute value of the difference between the times in which the same trigger is sent to both MEG and EEG systems and continuously increases over time: from low (delta = 0 ms) to high (delta = 197 ms) values. Correction of the linear drift estimated using a polynomial function to be applied to the signals is displayed with a blue dashed line. Corrected drift (delta ~0 ms over time) representing a synchronized time between MEG and EEG systems is displayed with a red dashed line. *Right panel*: Graphical representation of the time shift (delta = 197 ms) estimated for the last trigger sent to both MEG and EEG systems is displayed. Please click here to view a larger version of this figure.

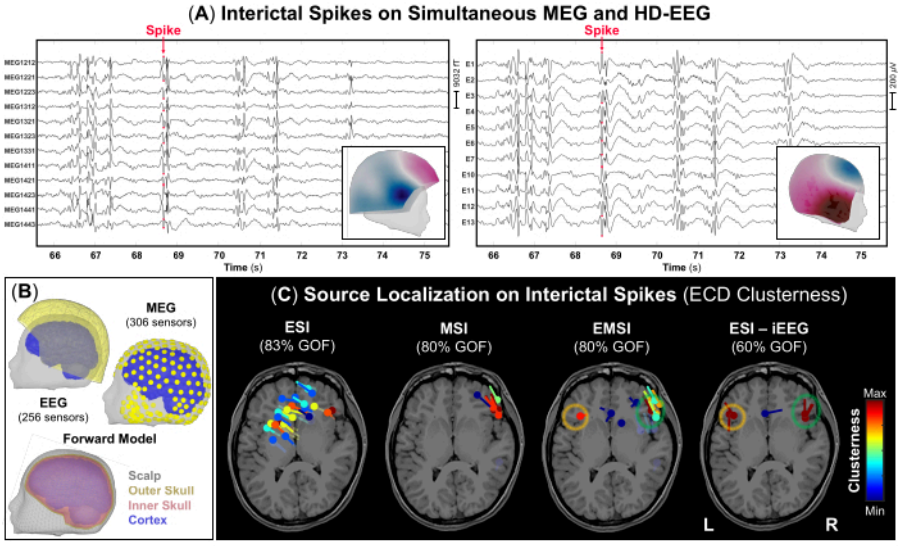

Figure 3: Interictal epileptiform discharges (IEDs) on MEG and HD-EEG data. (**A**) Time portion of simultaneous MEG and HD-EEG recording (10 s) from a 10-year-old female (Case 1) with frequent IEDs. A subgroup of the 306 MEG sensors and 256 EEG electrodes has been selected for visualization purposes. Topography field and potential maps at the peak of an IED are displayed as inner panels for MEG and HD-EEG, respectively. (**B**) Location of MEG and HD-EEG sensors (yellow-colored) coregistered on subject's 3D head and cortical (blue-colored) surfaces. Realistic boundary element method (BEM) head model consisting of three layers [i.e., scalp (grey-colored), outer skull (yellow-colored), and inner skull (pink-colored)] reconstructed from the pre-operative MRI of the subject. (**C**) Source localization clusterness results performed on IEDs using equivalent current dipole (ECD) are shown on subject's pre-operative MRI for ESI, MSI, EMSI, and ESI on iEEG (gold standard)[52]. Heat maps of dipole clusterness with a goodness-of-fit >60% are displayed from lower (blue) to higher (red) values. The seizure onset zone defined through ESI performed on iEEG data was regarded as the gold standard (orange and green circles). Please click here to view a larger version of this figure.

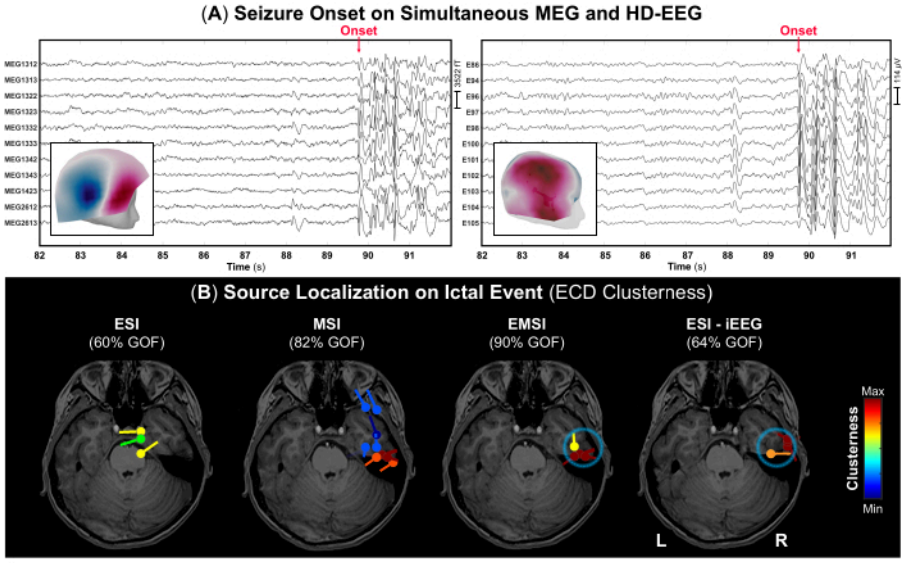

Figure 4: Seizure onset on MEG and HD-EEG data. (**A**) Time portion of simultaneous MEG and HD-EEG recording (10 s) from a 13-year-old male (Case 2) with the seizure onset (red arrow). A subgroup of the 306 MEG sensors and 256 EEG electrodes has been selected for visualization purposes. Topography field and potential maps at the ictal onset are displayed as inner panels for MEG and HD-EEG, respectively. (**B**) Source localization clusterness results performed at the onset of the ictal event using the equivalent current dipole (ECD) method are shown on the pre-operative MRI of the subject for ESI, MSI, EMSI, and ESI on iEEG (gold standard)[52]. Heat maps of dipole clusterness with a goodness-of-fit >60% are displayed from lower (blue) to higher (red) values. The seizure onset zone defined through ESI performed on iEEG data was regarded as gold standard (blue circle). Please click here to view a larger version of this figure.

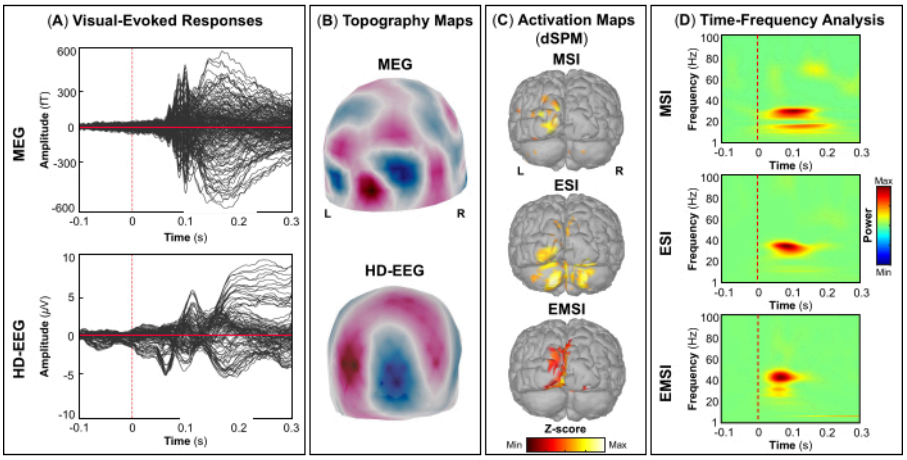

Figure 5: Visual-evoked fields and potentials from MEG and HD-EEG data. (**A**) Averaged visual-evoked responses of a 15-year-old female for MEG (top panel) and HD-EEG (bottom panel) are displayed for the time interval between -100 ms and 300 ms. (**B**) Topography field and potential maps of the primary visual cortex are displayed for MEG and HD-EEG, respectively. (**C**) Source activation maps with maximum amplitudes of cortical activation at brain regions of the Desikan-Killiany atlas (namely, cuneus and lateral occipital cortex) estimated using dynamic statistical parametric mapping (dSPM) method for MSI, ESI, and EMSI, respectively. Heat maps of the source activation (dSPM normalized z-score) are displayed. (**D**) Time-frequency maps obtained using Morlet wavelet time-frequency decomposition on the visual-evoked responses at the primary visual cortex are displayed for the -100 ms to 300 ms time window. Heat maps of the time-frequency power, expressed in percentages based on the deviation of the normalized data from the mean over the baseline [-200; 0] ms, are displayed. Please click here to view a larger version of this figure.

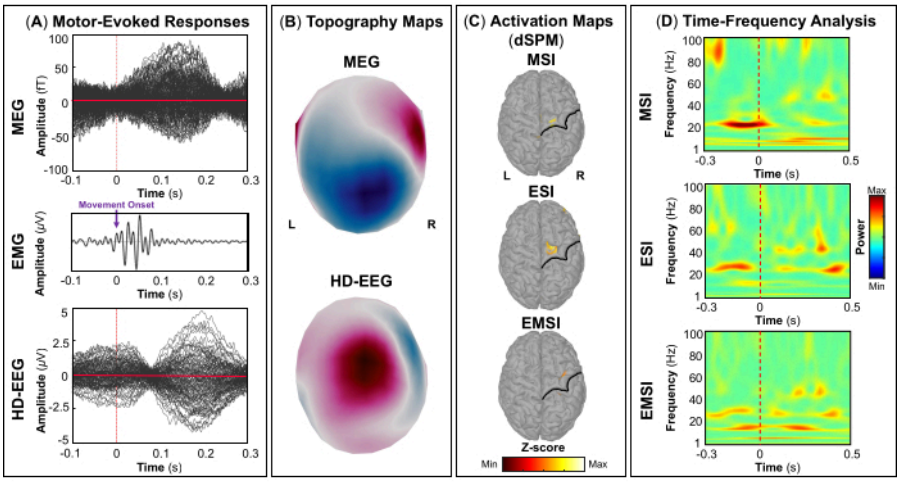

Figure 6: Motor-evoked fields and potentials from MEG and HD-EEG data. (**A**) Averaged motor-evoked responses of a 15-year-old female for MEG (top panel) and HD-EEG (bottom panel) are displayed for the left index-tapping task in the time-interval between -100 and 300 ms. The electromyography (EMG) signal (middle panel) with the movement onset (purple arrow) is displayed for the time-interval between -100 ms and 300 ms; the signal is filtered in the frequency band 30-300 Hz (Notch filter: 60 Hz). (**B**) Topography field and potential maps of the primary motor cortex are displayed for MEG and HD-EEG, respectively. (**C**) Source activation maps with maximum amplitudes of cortical activation at the contralateral precentral gyrus of the Desikan-Killiany atlas estimated using dynamic statistical parametric mapping (dSPM) method for MSI, ESI, and EMSI, respectively. Heat maps of the source activation (dSPM normalized z-score) are displayed, together with the central sulcus (black line). (**D**) Time-frequency maps obtained using Morlet wavelet time-frequency decomposition on the motor-evoked responses at the primary motor cortex for the -300 ms to 500 ms time window. Heat maps of the time-frequency power, expressed in percentages based on the deviation of the normalized data from the mean over the baseline [-1500; -1000] ms, are displayed. Please click here to view a larger version of this figure.

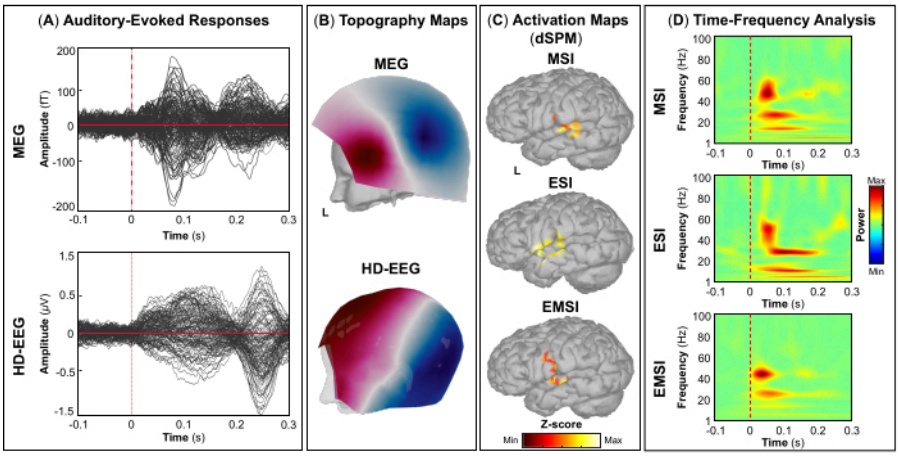

Figure 7: Auditory-evoked fields and potentials from MEG and HD-EEG data. (**A**) Averaged auditory-evoked responses of a 15-year-old female for MEG (top panel) and HD-EEG (bottom panel) are displayed for the time interval between -100 ms and 300 ms. (**B**) Topography field and potential maps of the primary auditory cortex are displayed for the MEG and HD-EEG, respectively. (**C**) Source activation maps with maximum amplitudes of cortical activation at the transverse temporal gyrus and posterior portion of the superior temporal gyrus of the Desikan-Killiany atlas estimated using dynamic statistical parametric mapping (dSPM) method for MSI, ESI, and EMSI, respectively. Heat maps of the source activation (dSPM normalized z-score) are displayed. (**D**) Time-frequency maps obtained using Morlet wavelet time-frequency decomposition on the auditory-evoked responses at the primary auditory cortex for the -100 to 300 ms time window. Heat maps of the time-frequency power, expressed in percentages based on the deviation of the normalized data from the mean over the baseline [-500; 0] ms, are displayed. Please click here to view a larger version of this figure.

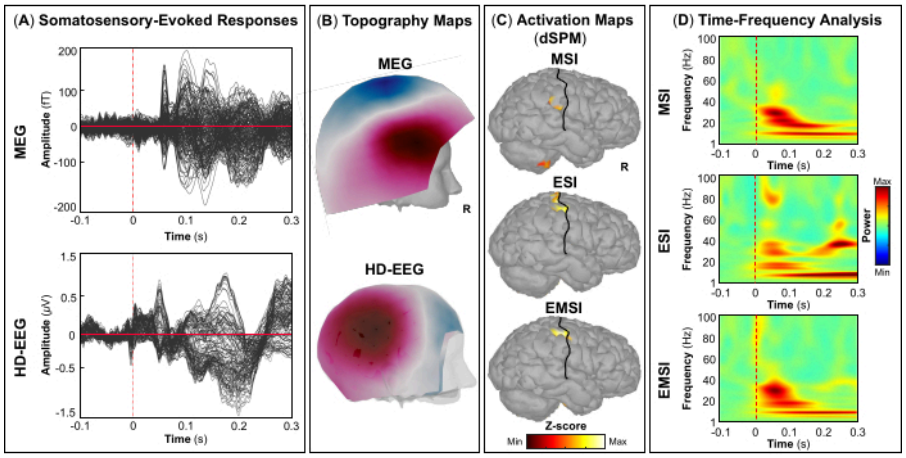

Figure 8: Somatosensory-evoked fields and potentials from MEG and HD-EEG data. (**A**) Averaged somatosensory-evoked responses of a 15-year-old female for MEG (top panel) and HD-EEG (bottom panel) are displayed for the left digits' stimulation in the time interval between -100 and 300 ms. (**B**) Topography field and potential maps of the primary somatosensory cortex are displayed for the MEG and HD-EEG, respectively. (**C**) Source activation maps with maximum amplitudes of cortical activation at the contralateral postcentral gyrus of the Desikan-Killiany atlas estimated using dynamic statistical parametric mapping (dSPM) method for MSI, ESI, and EMSI, respectively. Heat maps of the source activation (dSPM normalized z-score) are displayed, together with the central sulcus (black line). (**D**) Time-frequency maps obtained using Morlet wavelet time-frequency decomposition on the somatosensory-evoked responses at the primary somatosensory cortex for the -100 ms to 300 ms time window. Heat maps of the time-frequency power, expressed in percentages based on the deviation of the normalized data from the mean over the baseline [-100; 0] ms, are displayed. Please click here to view a larger version of this figure.

Discussion

In this study, we illustrate the experimental setup to record simultaneous MEG and HD-EEG in children with DRE while resting/sleeping, performing a task, or receiving stimuli, and propose a methodological framework for localizing the irritative zone, SOZ, and eloquent brain areas using EMSI, as well as individual MSI and ESI. We further provide technical recommendations for merging MEG and HD-EEG data from different commercially available products that present unique features. We present data from three cases to enhance the clinical utility of EMSI in the localization of epileptogenic and eloquent brain areas. The findings here indicate that EMSI results outperform those obtained by either modality alone, most likely due to the additive value of the complementary properties of MEG and EEG signals in the combined solution and possibly due to the increased number of sensors used for recording the data (>550 sensors). Particularly, EMSI noninvasively localized the irritative and SOZs with concordant findings as ESI on iEEG gold standard, which confirmed the clinical observations.

The proposed methodology includes the following critical steps: (i) high-quality acquisition of simultaneous MEG and HD-EEG (i.e., high SNR) recordings with high spatial sampling of sensors (>550 sensors) covering the entire brain of interictal and ictal activities, as well as visual-, motor-, auditory-, and somatosensory-evoked fields and potentials, from children with DRE (steps 3.1-3.2); (ii) temporal synchronization and spatial co-registration of MEG and HD-EEG signals recorded with different acquisition systems (step 3.12); (iii) careful preprocessing and selection of data portions containing interictal activity (steps 4.1.1-4.1.7), ictal onset activity (steps 4.2.1-4.2.7), and event-related responses (steps 4.3.1-4.3.6), respectively; and (iv) accurate source localization of the irritative zone, SOZ, and eloquent brain areas of interest using reliable source localization methods (e.g., ECDs with clustering and dSPM) (steps 4.1.8-4.1.9, 4.2.8-4.2.9, and 4.3.7-4.3.9, respectively).

The most critical step when performing simultaneous MEG and HD-EEG recordings is to spatially (alignment between coordinate spaces) and temporally (correction of the linear clock drift) synchronize the data recorded by the two acquisition systems. Such synchronization is crucial to ensure the correct identification of interictal, ictal, and visual/motor/auditory/tactile events that simultaneously occur in the MEG and HD-EEG signals. Errors in the timepoint selection of these events may affect the source localization results and identify areas of the brain that are not necessarily involved in the generation of these events.

MEG systems often offer compatible 32-, 64-, and 128-channel EEG systems incorporated into the product for performing simultaneous MEG and EEG measurements. In these cases, there is no need to temporally synchronize the data by sending common trigger signals. Similarly, most EEG systems are nowadays compatible with all MEG systems. Despite these advances in hardware, only few epilepsy centers perform simultaneous MEG and HD-EEG recordings as part of the presurgical evaluation. Here, we took advantage of such integrability and combined the 306-channel MEG and 256-channel EEG systems to simultaneously record the brain activity with >550 sensors covering the subject's head. So far, few software for advanced analysis of MEG, HD-EEG, and iEEG data (e.g., *Brainstorm*, *CURRY*, *EEGLab*, *FieldTrip*, *MNE*, or *NUTMEG*) are available. Future studies are therefore necessary to validate the proposed methodology with new neuroimaging analysis software. Finally, the combination of MSI and ESI into a unique solution (EMSI) increased the computational complexity of the data analysis.

The described method presents a few limitations that should be addressed in future studies. We manually selected IEDs occurring on both MEG and HD-EEG data of two representative patients while ignoring interictal spikes that occurred in only one of the two signals (either MEG or EEG). Manual selection of spikes can be a time-consuming and subjective approach that can be simplified using automated approaches for detecting IEDs developed during the last decades[57,58,59]. However, visual inspection is always recommended for careful analysis and refined detection of each IED. Furthermore, we used the SOZ as an approximator of the EZ. Yet, the SOZ does not always predict surgical outcomes[60,61,62,63]. Future studies can, therefore, use the surgical outcome as ground truth for more precise delineation of the EZ[13,14,15,16,17,19,20]. Although seizures can be successfully captured using simultaneous MEG and EEG and localized using appropriate source localization techniques[44,64], it is relatively rare to record such ictal events in clinical practice, especially from outpatients on ASMs. This is mostly due to the limited duration of MEG recordings and

the excessive body movements occurring during seizures (e.g., the patient's head slipped out the dewar), which may cause biological artifacts that can severely affect source localization findings. In a recent review, Stefan et al. reported the occurrence of seizures during MEG recordings in 7%-24% of patients, with an average recording time of 30 minutes up to 5.7 h across different studies[65]. At CCMC, 18 out of 89 (20.2%) patients had ictal events captured during simultaneous MEG and HD-EEG recordings performed within the past ~2 years. However, only 8 out of the 18 (44.4%) patients were successfully analyzed. In cases where interictal MEG recordings show normal or inconclusive findings, ictal MEG or HD-EEG may be used to localize the EZ with high precision. Yet, technical and logistical requirements for these recordings should be addressed. In addition, the representative data for the eloquent cortex localization via EMSI were not compared with any gold standards for localization of these functional brain areas, such as noninvasive fMRI or intraoperative electrocortical stimulation. Further investigations may, therefore, integrate EMSI and fMRI towards a multimodal noninvasive imaging tool to improve the localization accuracy of these eloquent brain areas in children with DRE. This work may also be extended to localize other functional brain areas, such as the language-eloquent regions. Localization of language functions is of critical importance during the presurgical evaluation of patients with DRE to determine their surgical candidacy, plan the extent of surgical resection, and prevent permanent postoperative functional deficits[66]. Several noninvasive studies have shown that language mapping using MEG can provide concordant results, similar to the invasive Wada test, which is often regarded as the gold standard for identifying the dominant language hemisphere[67,68,69,70]. A recent study has proposed a multimodal approach in which the combination of different techniques (i.e., cortical stimulation mapping, high-gamma electrocorticography, fMRI, and transcranial magnetic stimulation) can provide mutual, confirmatory, and complementary information for presurgical language mapping[71]. Despite these advantages, mapping language areas is still challenging in pediatric patients who have cognitive, intellectual, and language barriers due to their age. Thus, more age-specific tasks and child-friendly setups should be developed in the near future. In this work, we analyzed MEG and HD-EEG data using software that is not certified for clinical purposes. Although these tools have been proven to be valuable and effective, they carry liability issues that should be considered when reporting presurgical evaluation findings for clinical use. Here, we describe procedures for HD-EEG recordings using only sponge-based EEG electrode systems. Alternative systems using gel-based EEG electrodes are widely used in both clinical and research settings. Although they provide higher SNR EEG recordings, they required longer preparation time (~40-60 min) and thus are less suitable for pediatric use. Alternatively, several laboratories use low-density gel-based EEG systems during the MEG recordings, which are advantageous in terms of preparation time (compared to HD-EEG systems), but they offer significantly lower spatial resolution due to the reduced number of electrodes covering the entire scalp[12,16,72,73].

At present, the localization of the epileptogenic brain areas in patients with epilepsy is still mainly achieved with iEEG monitoring. Moreover, the methodology for the precise localization of eloquent brain areas is poorly defined, and the experiment setups currently used in MEG laboratories are inappropriate for pediatric patients, while the use of HD-EEG for this purpose is very limited. Accurate localization of these areas may facilitate the presurgical evaluation and augment the surgical planning for either resection or iEEG

electrode placement. So far, several studies investigated the contribution of either ESI or MSI in the presurgical evaluation of patients with DRE and focal epilepsies for the identification of the EZ[12,13,14,15,16,17,18,19] and eloquent areas of the somatosensory cortex[41], respectively. Few studies have shown better source localization results and outcome prediction performance using EMSI compared to either MSI or ESI alone[13,31,42]. Despite these findings, recording of MEG and EEG is rarely performed simultaneously, and MSI and ESI are implemented in only a few epilepsy centers worldwide. To our best knowledge, this is the first study that provides suggestions for collecting and analyzing simultaneous MEG and HD-EEG data, as well as performing EMSI in pediatric epilepsy for the noninvasive identification of the irritative zone, SOZ, and eloquent brain areas, namely primary visual, motor, auditory, and somatosensory cortices.

Here, we performed EMSI on interictal spikes and ictal events detected on simultaneous noninvasive data from two patients with DRE (Cases 1 and 2) and achieved a source localization error of ~9 mm and ~12 mm from the SOZ, respectively, in line with previous studies[42]. Impressively, such a method achieved a localization accuracy comparable to the intracranial findings (i.e., ESI on iEEG data), with clustered dipoles localized in the brain area pinpointed as epileptogenic by the clinical observations (**Figure 3C** and **Figure 4B**). Using noninvasive data from a third representative patient with DRE (Case 3), we also performed EMSI on visual-, motor-, auditory-, and somatosensory-evoked activities and found prominent source activation patterns in the corresponding eloquent brain areas (i.e., visual, motor, auditory, and somatosensory cortices) (**Figure 5C**, **Figure 6C**, **Figure 7C**, and **Figure 8C**).

Our results were derived from the fusion of complementary information captured from MEG and EEG modalities that may improve localization accuracy. EEG is well known to reflect all intracranial currents, whereas MEG is mostly sensitive to tangential sources and blind to deep brain sources[29,74]. As shown in this study, combining MEG and EEG can, therefore, overcome the limitations of each modality, provide superior localization results, and identify epileptogenic and eloquent brain areas that either ESI or MSI may have missed if used alone. Moreover, we present an alternative noninvasive approach for mapping eloquent brain areas using EMSI in those patients who did not undergo fMRI during their presurgical evaluation.

The localization of epileptogenic and eloquent brain areas using noninvasive techniques, such as simultaneous MEG and EEG, is an essential step during the presurgical evaluation of children with DRE for complete removal or disconnection of the EZ while preserving eloquent cortical areas. The proposed methodology offers a detailed description of the acquisition and analysis of simultaneous MEG and EEG data that supports its application not only in the presurgical epilepsy evaluation but also in cognitive neurosciences for exploring physiological functions of the healthy brain in both typically developing children as well as healthy adults, as well as morphological and functional brain changes associated with epilepsy or other neurological disorders. Future studies investigating epileptogenic brain networks may also assess whether network hubs (i.e., highly connected brain regions) estimated noninvasively using EMSI on simultaneous MEG and HD-EEG data can more accurately localize the EZ in children with DRE than those estimated using MSI and/or ESI alone[75,76,77]. Furthermore, the noninvasive mapping of spatiotemporal propagations of spikes and ripples (i.e., high-frequency oscillations, >80 Hz),

estimated through EMSI, can help to better understand the pathophysiological mechanisms of propagating epileptiform activity and noninvasively assess the onset generator of these propagations that is a precise biomarker of the EZ[78,79]. The presented protocol may help to further investigate the complementarity of MEG and EEG systems by examining the sensitivity of MEG and EEG sensor arrays to sources of different orientations. Such analysis may provide insights into the electrophysiological properties of the brain while performing simultaneous MEG and HD-EEG.

Disclosures

The authors report no disclosures.

Acknowledgments

This work was supported by the National Institute of Neurological Disorders and Stroke (R01NS104116; R01NS134944; Principal Investigator: Christos Papadelis).

References

1. Oldham, M. S., Horn, P. S., Tsevat, J., Standridge, S. Costs and clinical outcomes of epilepsy surgery in children with drug-resistant epilepsy. *Pediatr Neurol.* **53** (3), 216-220 (2015).
2. Willie, J. T. et al. Real-time magnetic resonance-guided stereotactic laser amygdalohippocampotomy for mesial temporal lobe epilepsy. *Neurosurgery.* **74** (6), 569-584 (2014).
3. Rosenow, F., Lüders, H. Presurgical evaluation of epilepsy. *Brain.* **124** (Pt 9), 1683-1700 (2001).
4. Önal, Ç. et al. Complications of invasive subdural grid monitoring in children with epilepsy. *J Neurosurg.* **98** (5), 1017-1026 (2003).
5. Hader, W. J. et al. Complications of epilepsy surgery-a systematic review of focal surgical resections and invasive EEG monitoring. *Epilepsia.* **54** (5), 840-847 (2013).
6. Meng, Y. et al. Risk factors for surgical site infection after intracranial electroencephalography monitoring for epilepsy in the pediatric population. *J Neurosurg Pediatr.* **22** (1), 31-36 (2018).
7. Jobst, B. C. et al. Intracranial EEG in the 21st Century. *Epilepsy Curr.* **20** (4), 180-188 (2020).
8. Schwartz, E. S. et al. Magnetoencephalography for pediatric epilepsy: how we do it. *AJNR Am J Neuroradiol.* **29** (5), 832-837 (2008).
9. Michel, C. M. et al. Electric source imaging of human brain functions. *Brain Res Rev.* **36** (2-3), 108-118 (2001).
10. Michel, C. M., He, B. EEG source localization. *Handb Clin Neurol.* **160**, 85-101 (2019).
11. Michel, C. M., Brunet, D. EEG source imaging: A practical review of the analysis steps. *Front Neurol.* **10**, 325 (2019).
12. Plummer, C. et al. Interictal and ictal source localization for epilepsy surgery using high-density EEG with MEG: a prospective long-term study. *Brain.* **142** (4), 932-951 (2019).
13. Duez, L. et al. Electromagnetic source imaging in presurgical workup of patients with epilepsy: A prospective study. *Neurology.* **92** (6), e576-e586 (2019).
14. Mouthaan, B. E. et al. Diagnostic accuracy of interictal source imaging in presurgical epilepsy evaluation: A systematic review from the E-PILEPSY consortium. *Clin Neurophysiol.* **130** (5), 845-855 (2019).

15. Pellegrino, G. et al. Clinical yield of magnetoencephalography distributed source imaging in epilepsy: A comparison with equivalent current dipole method. *Hum Brain Mapp.* **39** (1), 218-231 (2018).

16. Tamilia, E. et al. Assessing the localization accuracy and clinical utility of electric and magnetic source imaging in children with epilepsy. *Clin Neurophysiol.* **130** (4), 491-504 (2019).

17. Coito, A. et al. Interictal epileptogenic zone localization in patients with focal epilepsy using electric source imaging and directed functional connectivity from low-density EEG. *Epilepsia Open.* **4** (2), 281-292 (2019).

18. Singh, J., Ebersole, J. S., Brinkmann, B. H. From theory to practical fundamentals of electroencephalographic source imaging in localizing the epileptogenic zone. *Epilepsia.* **63** (10), 2476-2490 (2022).

19. Brodbeck, V. et al. Electrical source imaging for presurgical focus localization in epilepsy patients with normal MRI. *Epilepsia.* **51** (4), 583-591 (2010).

20. Santalucia, R. et al. Clinical added value of interictal automated electrical source imaging in the presurgical evaluation of MRI-negative epilepsy: A real-life experience in 29 consecutive patients. *Epilepsy Behav.* **143**, 109229 (2023).

21. Schneider, F. et al. Magnetic source imaging in non-lesional neocortical epilepsy: additional value and comparison with ICEEG. *Epilepsy Behav.* **24** (2), 234-240 (2012).

22. Hämäläinen, M., Hari, R., Ilmoniemi, R. J., Knuutila, J., Lounasmaa, O. V. Magnetoencephalography-theory, instrumentation, and applications to noninvasive studies of the working human brain. *Rev Mod Phys.* **65**, 413-497 (1993).

23. Baillet, S., Mosher, J. C., Leahy, R. M. Electromagnetic brain mapping. *IEEE Signal Process Mag.* **18** (6), 14-30 (2001).

24. Fuchs, M., Kastner, J., Tech, R., Wagner, M., Gasca, F. MEG and EEG dipole clusters from extended cortical sources. *Biomed Eng Lett.* **7** (3), 185-191 (2017).

25. Singh, S. P. Magnetoencephalography: Basic principles. *Ann Indian Acad Neurol.* **17** (Suppl 1), S107 -S112 (2014).

26. Ahlfors, S. P., Han, J., Belliveau, J. W., Hämäläinen, M. S. Sensitivity of MEG and EEG to source orientation. *Brain Topogr.* **23**, 227-232 (2010).

27. Kim, H., Chung, C. K., Hwang, H. Magnetoencephalography in pediatric epilepsy. *Korean J Pediatr.* **56** (10), 431-438 (2013).

28. Gorjan, D., Gramann, K., De Pauw, K., Marusic, U. Removal of movement-induced EEG artifacts: Current state of the art and guidelines. *J Neural Eng.* (2022).

29. Barkley, G. L., Baumgartner, C. MEG and EEG in epilepsy. *J Clin Neurophysiol.* **20** (3), 163-178 (2003).

30. Ebersole, J. S., Ebersole, S. M. Combining MEG and EEG source modeling in epilepsy evaluations. *J Clin Neurophysiol.* **27** (6), 360-371 (2010).

31. Yoshinaga, H. et al. Benefit of simultaneous recording of EEG and MEG in dipole localization. *Epilepsia.* **43** (8), 924-928 (2002).

32. Baumgartner, C. Controversies in clinical neurophysiology. MEG is superior to EEG in the localization of interictal epileptiform activity: Con. *Clin Neurophysiol.* **115** (5), 1010-1020 (2004).

33. Barkley, G. L. Controversies in neurophysiology. MEG is superior to EEG in localization of interictal epileptiform activity: Pro. *Clin Neurophysiol.* **115** (5) 1001-1009 (2004).
34. Braeutigam, S. Magnetoencephalography: Fundamentals and established and emerging clinical applications in radiology. *ISRN Radiol.* **2013**, 529463 (2013).
35. Papadelis, C. et al. Current and emerging potential for magnetoencephalography in pediatric epilepsy. *J Pediatr Epilepsy.* **2** (1), 73-85 (2013).
36. Fiedler, P., Fonseca, C., Supriyanto, E., Zanow, F., Haueisen, J. A high-density 256-channel cap for dry electroencephalography. *Hum Brain Mapp.* **43** (4), 1295 (2022).
37. Sharon, D., Hämäläinen, M. S., Tootell, R. B. H., Halgren, E., Belliveau, J. W. The advantage of combining MEG and EEG: comparison to fMRI in focally-stimulated visual cortex. *Neuroimage.* **36** (4), 1225 (2007).
38. Pataraia, E., Lindinger, G., Deecke, L., Mayer, D., Baumgartner, C. Combined MEG/EEG analysis of the interictal spike complex in mesial temporal lobe epilepsy. *Neuroimage.* **24** (3), 607-614 (2005).
39. Ahmed Mahmutoglu, M., Rupp, A., Baumgärtner, U. Simultaneous EEG/MEG yields complementary information of nociceptive evoked responses. *Clin Neurophysiol.* **143**, 21-35 (2022).
40. Aydin, Ü. et al. Combined EEG/MEG can outperform single modality EEG or MEG source reconstruction in presurgical epilepsy diagnosis. *PLoS One.* **10** (3), e0118753 (2015).
41. Bast, T. et al. Combined EEG and MEG analysis of early somatosensory evoked activity in children and adolescents with focal epilepsies. *Clin Neurophysiol.* **118** (8), 1721-1735 (2007).
42. Chikara, R. K. et al. Electromagnetic source imaging predicts surgical outcome in children with focal cortical dysplasia. *Clin Neurophysiol.* **153**, 88-101 (2023).
43. Hari, R. et al. IFCN-endorsed practical guidelines for clinical magnetoencephalography (MEG). *Clin Neurophysiol.* **129** (8), 1720-1747 (2018).
44. Bagić, A. I., Knowlton, R. C., Rose, D. F., Ebersole, J. S. American Clinical Magnetoencephalography Society Clinical Practice Guideline 1: Recording and analysis of spontaneous cerebral activity. *J Clin Neurophysiol.* **28** (4), 348-354 (2011).
45. Papadelis, C., Chen, Y. H. Pediatric magnetoencephalography in clinical practice and research. *Neuroimaging Clin N Am.* **30** (2), 239-248 (2020).
46. De Macedo Rodrigues, K. et al. A FreeSurfer-compliant consistent manual segmentation of infant brains spanning the 0-2 year age range. *Front Hum Neurosci.* **9**, 21 (2015).
47. Tadel, F., Baillet, S., Mosher, J. C., Pantazis, D., Leahy, R. M. Brainstorm: A user-friendly application for MEG/EEG analysis. *Comput Intell Neurosci.* **2011**, 879716 (2011).
48. Kane, N. et al. A revised glossary of terms most commonly used by clinical electroencephalographers and updated proposal for the report format of the EEG findings. Revision 2017. *Clin Neurophysiol Pract.* **2**, 170-185 (2017).

49. Lantz, G. et al. Propagation of interictal epileptiform activity can lead to erroneous source localizations: a 128-channel EEG mapping study. *J Clin Neurophysiol.* **20** (5), 311-319 (2003).

50. Vorwerk, J. et al. A guideline for head volume conductor modeling in EEG and MEG. *Neuroimage.* **100**, 590-607 (2014).

51. Schrader, S. et al. DUNEuro-A software toolbox for forward modeling in bioelectromagnetism. *PLoS One.* **16** (6), e0252431 (2021).

52. Ntolkeras, G. et al. Presurgical accuracy of dipole clustering in MRI-negative pediatric patients with epilepsy: Validation against intracranial EEG and resection. *Clin Neurophysiol.* **141**, 126-138 (2022).

53. David, O., Kilner, J. M., Friston, K. J. Mechanisms of evoked and induced responses in MEG/EEG. *Neuroimage.* **31**, 1580-1591 (2006).

54. Pantev, C. Evoked and induced gamma-band activity of the human cortex. *Brain Topogr.* **7** (4), 321-330 (1995).

55. Fox, N. A. et al. Assessing human mirror activity with EEG mu rhythm: A meta-analysis. *Psychol Bull.* **142** (3), 291-313 (2016).

56. Genzer, S., Ong, D. C., Zaki, J., Perry, A. Mu rhythm suppression over sensorimotor regions is associated with greater empathic accuracy. *Soc Cogn Affect Neurosci.* **17** (9), 788-801 (2022).

57. Janmohamed, M. et al. Moving the field forward: detection of epileptiform abnormalities on scalp electroencephalography using deep learning-clinical application perspectives. *Brain Commun.* **4** (5), fcac218 (2022).

58. Bagheri, E., Jin, J., Dauwels, J., Cash, S., Westover, M. B. A fast machine learning approach to facilitate the detection of interictal epileptiform discharges in the scalp electroencephalogram. *J Neurosci Methods.* **326**, 108362 (2019).

59. Thomas, J. et al. Automated detection of interictal epileptiform discharges from scalp electroencephalograms by convolutional neural networks. *Int J Neural Syst.* **30** (11), 2050030 (2020).

60. Zijlmans, M., Zweiphenning, W., van Klink, N. Changing concepts in presurgical assessment for epilepsy surgery. *Nat Rev Neurol.* **15** (10), 594-606 (2019).

61. Akiyama, T. et al. Focal resection of fast ripples on extraoperative intracranial EEG improves seizure outcome in pediatric epilepsy. *Epilepsia.* **52** (10), 1802-1811 (2011).

62. Duncan, J. S., Winston, G. P., Koepp, M. J., Ourselin, S. Brain imaging in the assessment for epilepsy surgery. *Lancet Neurol.* **15** (4), 420 (2016).

63. Jacobs, J. et al. High-frequency electroencephalographic oscillations correlate with outcome of epilepsy surgery. *Ann Neurol.* **67** (2), 209-220 (2010).

64. Ricci, L. et al. Virtual implantation using conventional scalp EEG delineates seizure onset and predicts surgical outcome in children with epilepsy. *Clin Neurophysiol.* **139**, 49-57 (2022).

65. Stefan, H., Rampp, S. Interictal and Ictal MEG in presurgical evaluation for epilepsy surgery. *Acta Epileptologica.* **2**, 11 (2020).

66. Jahangiri, F. R., Chima, G. S., Pearson, M., Jackson, J., Siddiqui, A. A. Mapping of the language cortex. *Cureus.* **13** (5), e14960 (2021).

67. Merrifield, W. S., Simos, P. G., Papanicolaou, A. C., Philpott, L. M., Sutherling, W. W. Hemispheric language dominance in magnetoencephalography: sensitivity, specificity, and data reduction techniques. *Epilepsy Behav.* **10** (1), 120-128 (2007).
68. Wheless, J. W. et al. Magnetoencephalography (MEG) and magnetic source imaging (MSI). *Neurologist.* **10** (3), 138-153 (2004).
69. Breier, J. I., Simos, P. G., Zouridakis, G., Papanicolaou, A. C. Lateralization of activity associated with language function using magnetoencephalography: a reliability study. *J Clin Neurophysiol.* **17** (5), 503-510 (2000).
70. Pataraia, E., Baumgartner, C., Lindinger, G., Deecke, L. Magnetoencephalography in presurgical epilepsy evaluation. *Neurosurg Rev.* **25** (3), 141-159 (2002).
71. Babajani-Feremi, A. et al. Language mapping using high gamma electrocorticography, fMRI, and TMS versus electrocortical stimulation. *Clin Neurophysiol.* **127** (3), 1822-1836 (2016).
72. Brodbeck, V. et al. Electroencephalographic source imaging: a prospective study of 152 operated epileptic patients. *Brain.* **134** (Pt 10), 2887-2897 (2011).
73. Sohrabpour, A. et al. Effect of EEG electrode number on epileptic source localization in pediatric patients. *Clin Neurophysiol.* **126** (3), 472-480 (2015).
74. Laohathai, C. et al. Practical fundamentals of clinical MEG interpretation in epilepsy. *Front Neurol.* **12**, 722986 (2021).
75. Corona, L. et al. Mapping functional connectivity of epileptogenic networks through virtual implantation. *Proceedings of the Annu Int Conf IEEE Eng Med Biol Soc.* **2021**, 408-411 (2021).
76. Corona, L. et al. Non-invasive mapping of epileptogenic networks predicts surgical outcome. *Brain.* **146** (5), 1916-1931 (2023).
77. Rijal, S. et al. Functional connectivity discriminates epileptogenic states and predicts surgical outcome in children with drug resistant epilepsy. *Sci Rep.* **13** (1), 9622 (2023).
78. Tamilia, E. et al. Noninvasive mapping of ripple onset predicts outcome in epilepsy surgery. *Ann Neurol.* **89** (5), 911-925 (2021).
79. Matarrese, M. A. G. et al. Spike propagation mapping reveals effective connectivity and predicts surgical outcome in epilepsy. *Brain.* **146** (9), 3898-3912 (2023).